ADVANCED MATERIALS
www.advmat.de

Recycling and Reusing of Graphite from Retired Lithium-ion Batteries: A Review

Honghong Tian, Magdalena Graczyk-Zajac,* Alois Kessler, Anke Weidenkaff, and Ralf Riedel*

The proliferation of rechargeable lithium-ion batteries (LIBs) over the past decade has led to a significant increase in the number of electric vehicles (EVs) powered by these batteries reaching the end of their lifespan. With retired EVs becoming more prevalent, recycling and reusing their components, particularly graphite, has become imperative as the world transitions toward electric mobility. Graphite constitutes ≈20% of LIBs by weight, making it a valuable resource to be conserved. This review presents an in-depth analysis of the current global graphite mining landscape and explores potential opportunities for the "second life" of graphitefrom depleted LIBs. Various recycling and reactivation technologies in both industry and academia are discussed, along with potential applications for recycled graphite forming a vital aspect of the waste management hierarchy. Furthermore, this review addresses the future challenges faced by the recycling industry in dealing with expired LIBs, encompassing environmental, economic, legal, and regulatory considerations. In conclusion, this review provides a comprehensive overview of the developments in recycling and reusing graphite from retired LIBs, offering valuable insights for forthcoming large-scale recycling efforts.

1. Introduction

Graphite is internationally utmost recognized as a "strategic resource to underpin the high technology development in the 21st century" due to its unparalleled electrical conductivity,[1] thermal conductivity,[2,3] lubricity,[4,5] high temperature and thermal shock resistance,[6,7] chemical stability[8] and plasticity.[9,10] Thus, graphite is omnipresent in a broad variety of products that has become an integral part of a human habitat (**Figure 1**). The commercial graphite chain includes upstream resource mining and beneficiation, midstream material grade product processing and downstream terminal applications, forming a multi-level graphite product system along the industry chain. Both upstream (low-end graphite) and midstream (mid-end graphite) have demonstrated excellent value in traditional industry segments such as steel and foundry. With the in-depth evolvement of physicochemical properties of graphite, downstream graphite (high-end graphite) such as spherical graphite, expanded graphite, graphene and other types of graphite are destined to penetrate into strategic industries such as renewable energy storage batteries, nuclear energy, aerospace, and medical care.[11] Demand of graphite has historically been driven by traditional refractory, foundry, crucible, electrodes and industrial applications, now and in future more by LIBs for EVs (**Figure 2**). The natural graphite demand by end-user applications rises drastically from 1069 thousand tonnes (kt) in 2016 to 1827 kt in 2023 and is expected to hit 4310 kt in 2030 (Figure 2a).[12]

Graphite, being a globally abundant non-metallic mineral raw material, is extensively distributed across many countries and regions worldwide. Nevertheless, nearly over 99% of the worldwide graphite resources are concentrated in ten countries including Turkey, China, Brazil, Madagascar, Mozambique, Tanzania, India, Uzbekistan, Canada, and Mexico. In 2022, global reserves of graphite were anticipated to be 323.6 million tonnes (Mt).[13] The pictorial overview of the global distribution and reserves of graphite mines in 2021 and 2022 is depicted in **Figure 3**. Turkey has the largest graphite reserves, accounting for 90 Mt of the 323.6 Mt in total, followed by Brazil with 74 Mt and China with 52 Mt in 2022. Together these three countries hold 66.7% of the forecasted world graphite reserves. In addition to these three nations, the majority of the world's large graphite projects which are currently under construction are concentrated in Mozambique, Tanzania, Canada, and Australia. The remaining part is mainly spread out among Vietnam, the Czech Republic, Sri Lanka,

H. Tian, M. Graczyk-Zajac, A. Weidenkaff, R. Riedel
Department of Materials and Earth Sciences
Technical University of Darmstadt
Otto-Berndt-Straße 3, 64287 Darmstadt, Germany
E-mail: honghong.tian@stud.tu-darmstadt.de;
m.graczyk-zajac@enbw.com
H. Tian, M. Graczyk-Zajac, A. Kessler
EnBW Energie Baden-Württemberg AG
Durlacher Allee 93, 76131 Karlsruhe, Germany
A. Weidenkaff
Fraunhofer Research Institution for Materials Recycling and Resource Strategy (IWKS)
Brentanostraße 2a, 63755 Alzenau, Germany

The ORCID identification number(s) for the author(s) of this article can be found under https://doi.org/10.1002/adma.202308494

DOI: 10.1002/adma.202308494

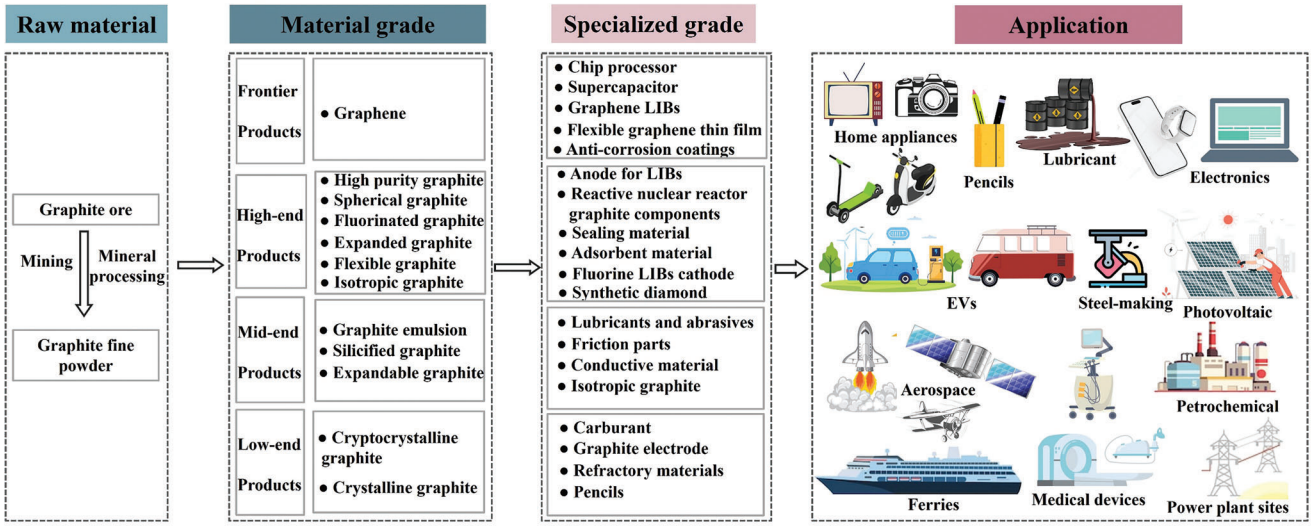

Figure 1. Graphite classification and application in human habitat (each small icon from www.freepik.com).[11]

Norway, Russia, Ukraine, and the United States. Graphite obtained from natural mining contains a high level of impurities, thereby requiring purification before it can be used. According to the United States Geological Survey, Madagascar, Mozambique and Tanzania are located in the East African Rift Valley geological belt, which is extremely rich in mineral resources. In 2021, these three countries ranked fourth to sixth in the world in terms of proven graphite reserves. The Barama ore in Mozambique, the Moro ore in Madagascar, and the Mahenge ore in Tanzania are examples of the massive reserves that have been recently discovered. More importantly, the minerals are of excellent quality, high purity, and large size in all three countries. Natural flake graphite deposits serve as the leading type of graphite deposits in the world. In the recent past, the annual production has been relatively stable at 1.1 Mt, except for 2017 and 2018 when it plummeted by ≈900 kt due to a series of factors.

Concerning graphite production, China, Brazil, Mozambique, and Madagascar account for ≈93% of global graphite production as shown in Figure 3, but the importance of Russia, South Korea, Canada, and Norway should not be underestimated.[13] Aoyu Graphite Group in China can produce microcrystalline graphite which is required in high-tech domain. In India, flake and powdered products are both provided by Agrawal Graphite Industries and T.P.Minerals Pvt Ltd. Flake graphite from Tamin Granites is mainly used for casting and crucible consumption. National De Grafite and Grafita MG Ltda. in Brazil are the two largest graphite producers in the world. Australia is a potential future graphite producer, notwithstanding there is no production yet. Balama ore in Australia, operated by Syrah Resources, has the largest high-grade natural flake graphite ore in terms of reserves. Asbury Carbons is the largest processor and exporter of natural graphite in the United States but has no graphite mines on its own and instead exports through a quantity of other graphite production facilities. Canada is the only country with graphite mining operations in North America, and Molo mine owned by Next Resources is one of the world's largest and highest quality flake graphite mines. Industrial Minerals is another big producer of flake crystalline graphite in North

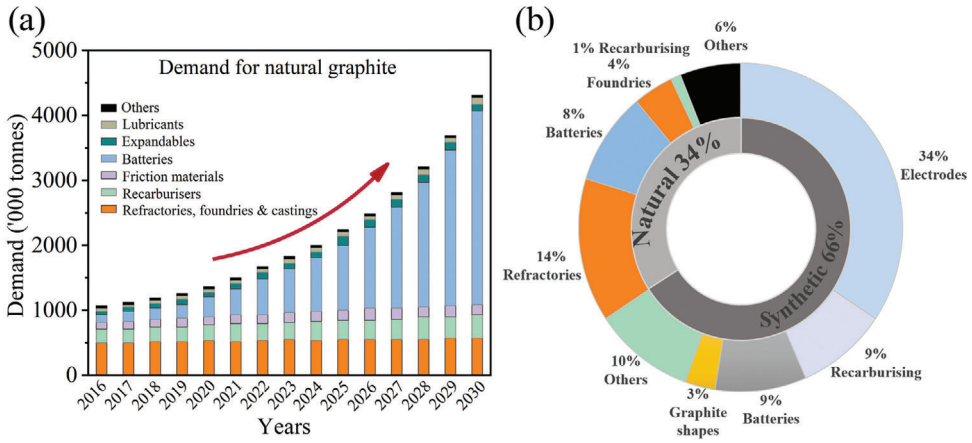

Figure 2. a) Global market analysis of natural graphite from 2016–2030.[12] b) This circular chart shows the major global uses of natural (34%) and synthetic (66%) graphite in 2021.

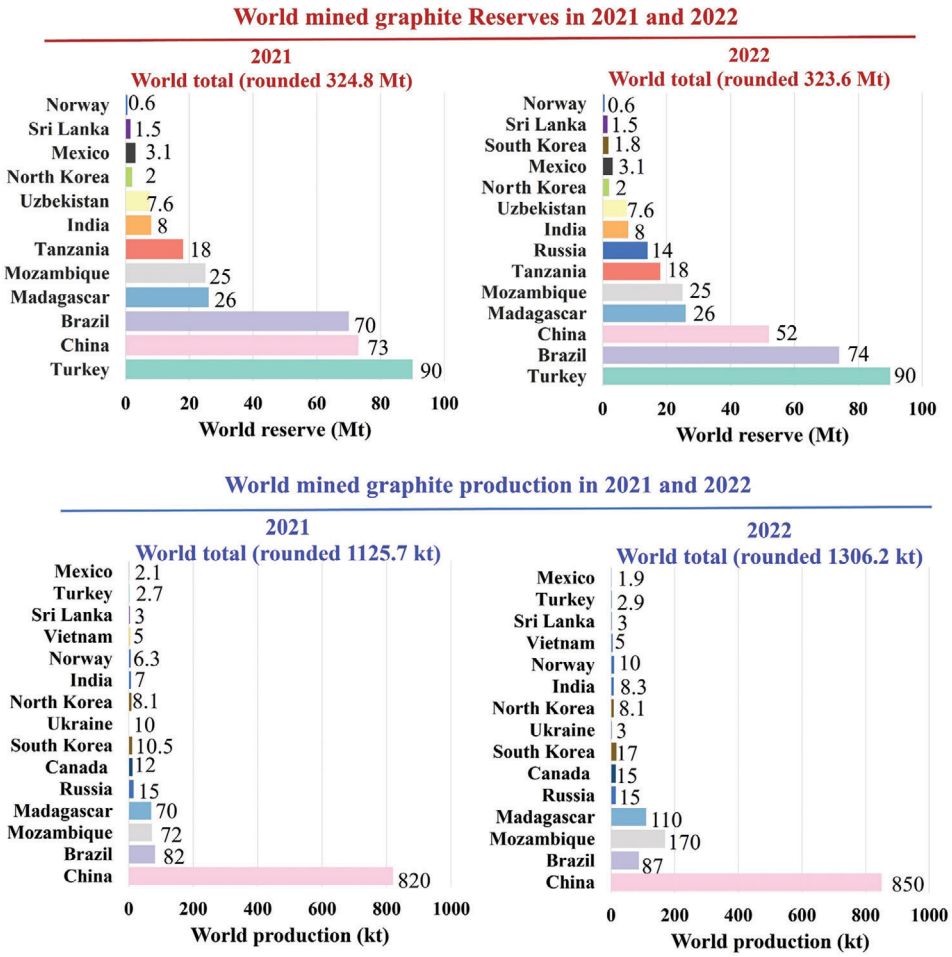

Figure 3. World mined graphite reserves and production in 2021 and 2022.[13]

America. Additionally, there are Graphite Kropfmühl AG in Germany, Grafitbergbau Kaisersberg GmbH in Austria, Mirab Mineral Resurer AB in Sweden, Skaland Graphite AS in Norway, two graphite producers in the Czech Republic, Koh-i-noor Grafit S.r.o. and Graphite Tyn spol.s.r.o. as well as Zavalievsky Gaphite Kombinat from Ukraine (**Table 1**). There are constraints in terms of the import and export prices of graphite products, such as China and Brazil mainly export low-end products, that is "inexpensive in export and expensive in imports".[14a] In contrast to Japan, U.S. and Germany manufacture high-quality products through sophisticated means of processing technology and sell them at high prices, i.e."low prices in imports and high prices in exports". The reality is that mining graphite typically results in graphite with a purity of less than 98%, and additional purification steps involving chemical and heat treatment are usually necessary to achieve the required electronic grade graphite purity of over 99.5% which can be used for anodes of LIBs.

Two sources of graphite for LIBs electrodes are natural graphite, sourced from mined graphite, and synthetic graphite, primarily manufactured using needle coke as the primary raw material. Needle coke is categorized in two types: petroleum and coal-tar pitch needle coke. Petroleum coke is a carbonaceous by-product of high-boiling hydrocarbon fractions obtained in petroleum refining, while coal-tar pitch is made from coal tar after its distillation that occurs during the coke production process. Those technologies and marketplaces have been monopolized by the United States, Japan, and the United Kingdom. Conoco INC Phillips 66 (plants in Lake Charles and Killingholme-Immingham) is the largest petroleum-based needle coke player in the world, with 55% market share and 420 kt production capacity per year as demonstrated in **Figure 4**. Japan can produce both coal-tar pitch and petroleum needle coke. The coal-tar pitch needle coke is only produced by Mitsubishi Chemical Corp. and Mitsubishi Chemical in Japan, and the proprietary technology is highly confidential. The largest competitors for Phillips 66 in the petroleum needle coke production share are Japanese players, such as Seadrift/GTI (plant in Port Lavaca) with 19% share, JX Nippon with 13% share, and Petrocokes Japan Ltd. with 13% share. C-Chem and Mitsubishi Chemical Corp. are currently the world's largest producers of coal-tar pitch needle coke with 900 kt per year and 800 kt per year capacity production, respectively. The consumption of needle coke edged upward due to the growth in the trajectory of LIBs. The demand was ≈800 kt in 2017 and is expected to boom to exceed 2500 kt in 2029.[15–17]

The global lithium-based rechargeable battery markets benefit from the booming automobile electrification, which is

Table 1. Important companies producing graphite around the world.[14]

Countries	Enterprises	Graphite type	Location, reserves, carbon content	Capacity (kt/year)	Mined life (year)
Australia	Syrah Resources	Flake	Balama, 16 900 kt	350	50+ [14b]
	Eagle Bay Resources	Flake	Australia, 6 000 kt, C 7.4%	–	. [14c]
	Black Rock Mining	All	Ulanga, 83 000 kt	340	16 [14d]
	Kibaran Resources	All	Epanko, 10 900 kt, C 8.6%	60	25 [14e]
China	Aoyu Graphite Group	Flake	Heilongjiang, 1 428 kt, C 12.7%	100	. [14c]
	Jixi Liumao Graphite Resources	Flake	Jixi, 21 100 kt, C 10.3%	80	. [14c]
Canada	Industrial Mineral Scanadainc.	Flake	Bisset Creek, C 94.7%	150	. [14c]
	Worldwide Graphite Producers Ltd.	Flake	Canada, 55 000 kt	–	. [14c]
	Quinto Mining Corp.	Flake	Canada	–	. [14c]
	Next Resources	Flake	Molo, 23 620 kt, C 6.32%	150	30 [14f]
	Timcal	Flake	Iles lake, C 94%–99%	20	. [14c]
Brazil	National De Grafite	Flake	Minas Gerais	70	. [14c]
	Grafita MG Ltda.	Flake	Minas Gerais	40	. [14c]
USA	Fortune Graphite Producers	Amorphous	Canada, C 95%	270	. [14c]
India	Tirupati Graphite	–	Montepuez, Barama, 15 200 kt, C 8.5%	100	. [14g]
Germany	Graphite Kropfmühl AG	All	Germany, China, Sri Lanka, UK, Zimbabwe	30	. [14c]
Austria	Grafitbergbau Kaisersberg GmbH	All	Kaysersberg, C 85–99.5%	30	. [14c]
Sweden	Mirab Mineral Resurer AB	Flake	Sweden, ≈7 000 kt, C 10%	1.30	. [14c]
Norway	Skaland Graphite AS	Flake	Norway, C 85–99%	1.20	. [14c]
Czech	Koh-I-Noor Grafit	Flake	Czech, Netolice, C 65–98%	–	. [14c]

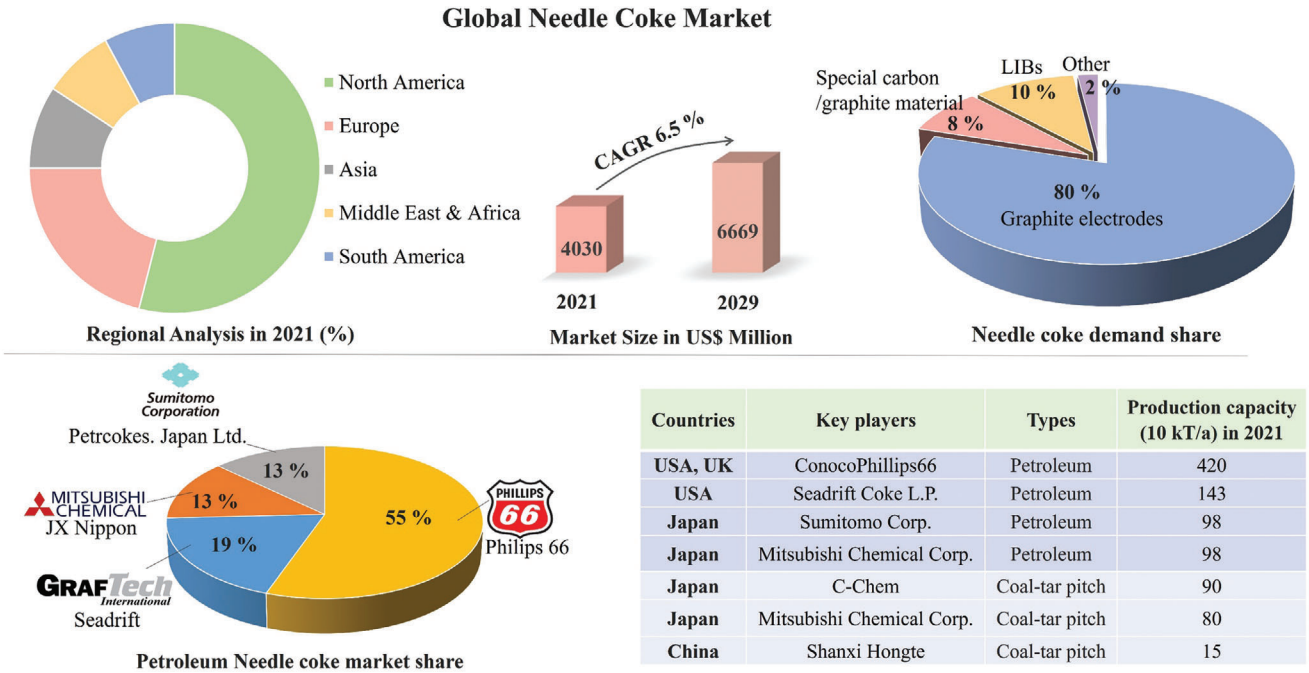

Countries	Key players	Types	Production capacity (10 kT/a) in 2021
USA, UK	ConocoPhillips66	Petroleum	420
USA	Seadrift Coke L.P.	Petroleum	143
Japan	Sumitomo Corp.	Petroleum	98
Japan	Mitsubishi Chemical Corp.	Petroleum	98
Japan	C-Chem	Coal-tar pitch	90
Japan	Mitsubishi Chemical Corp.	Coal-tar pitch	80
China	Shanxi Hongte	Coal-tar pitch	15

Figure 4. Needle coke market-global industry analysis and forecast.[15–17]

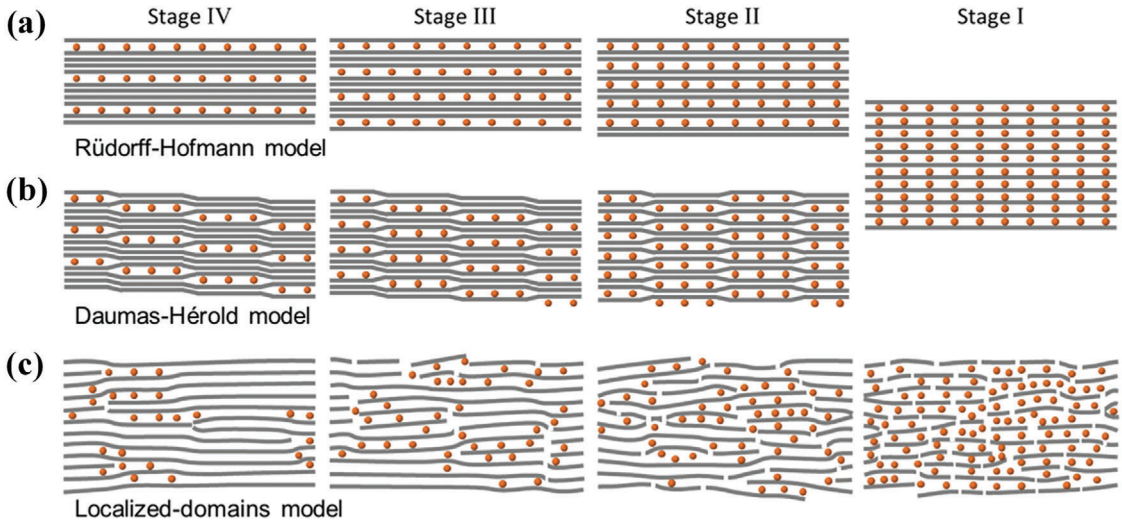

Figure 5. Schematic illustration of the lithiated graphite at different stages a) Rüdorff-Hofmann model. b) Daumas-Hérold model. c) Localized-domains mode. Reproduced (Adapted) with permission.[21] Copyright@2022, Wenzhou Univeristy and John Wiley & Sons Australia, Ltd.[21]

progressively accelerating due to the requirement to decarbonize personal transportation. The largest global power battery Megafactories are CATL, BYD, GXHT, CALB in China, LG Chem, Samsung SDI and SK Innovation in Korea, Panasonic, AESC, PEVE, LEJ in Japan, Northvolt in Sweden and Germany, SK Innovation in Hungary and Tesla in United States, all of them adopting mostly graphite (except for silicon/graphite composite or silicon/oxygen composite) as anode material. Global ownership of EVs would enlarge from ≈20 to 230 million by 2030, according to the International Energy Agency's.[18] Graphite is currently a universally accepted anode material due to its good long-term cycling performance and high intercalated lithium capacity (at low lithiation potential < 0.1 V vs Li^+/Li) and high electrical conductivity, as well as large lithium-ion diffusion coefficient, high tap density and relatively low volume change during lithiation/delithiation. Graphite undergoes a continuous phase transition during intercalation/deintercalation to form n≥ 2 kinetically or thermodynamically stable graphite intercalation compounds (GICs). There are currently three recognized reaction mechanisms for graphite intercalation compounds: (1) Rüdorff-Hofmann model indicates that lithium ions alternatively occupy the graphene layers for every four to one in the stage IV to I (LiC_{24} to LiC_6), but it is difficult to transfer them smoothly, suggesting that fast charging of graphite is impossible due to its own kinetic limitations;[19] (2) Daumas-Hérold model suggests that the lithium ions are able to adapt to graphene layers to deform or bulge during the intercalation process without significantly altering the structure of the graphite layers;[20] (3) Localized-Domains model proposes that the lithium ions are unevenly distributed between the graphite layers, generating localized stresses that lead to twisting and deformation of the graphite structure, and the formation of dislocations. The transformation between different order structures is realized by lithium ions diffusion and the movement, interaction and transformation of dislocations.[21] LiC_6 (Li-GIC) allows for the storage of up to 1 lithium atom per 6 C and is widely employed as anode material for commercial state-of-the-art LIBs due to the small radius of the lithium ions, which is one of the smallest known volume expansions of the 1st order GICs (LiC_6: theoretical capacity 372 mAh g^{-1} and 840 mAh cm^{-3} volumetric capacity) as demonstrated in **Figure 5**.

The current graphite anode material industry chain is dominated by China, with BTR and Shanshan being the world´s leading producer of natural graphite and synthetic graphite for LIBs anode materials, respectively.[22] It should be noted that the prices of the raw materials, petroleum-based coke and coal-based coke for manufacturing graphite anode, have remain relatively stable at 1100 \$ t^{-1} and 1340 \$ t^{-1} respectively. However, the price of pitch for coating graphite has seen a significant increase, from 1925 \$ t^{-1} to 2963 \$ t^{-1}. In the current market, artificial graphite is priced at 10 430 \$ t^{-1} (**Figure 6**a). With the anticipation of a surge in demand, particularly in EVs and stationary energy storage, the market of power battery and energy storage battery are expected to experience a remarkable demand growth, whereas the growth rate of the consumer battery market is projected to keep stable (Figure 6b). By 2025, the expected global demand for power batteries is estimated to exceed 1 TWh. Notably, a hybrid EV typically requires ≈10 kg graphite, whereas this requirement increases to ≈70 kg in a battery electric vehicle. Globally proven natural graphite reserves amount to ≈331 Mt by the end of 2021, and roughly speaking, the static guaranteed mining life anticipation of global graphite resources is ≈256 years.[13] However, the fact that graphite mines are mostly dense and massive in nature, coupled with the presence of impurity minerals (quartz, calcite, etc.) imposes complexity to the separation and selection processes, thereby driving up the cost of producing battery-grade graphite (with a target purity of ≥ 99.95%). Currently, the annual production of natural graphite stands at ≈1.2 Mt, of which 15–20% is utilized for manufacturing EV batteries.[22] To meet the growing demand for battery-grade graphite, it would be necessary to produce an additional 2.5-3 Mt of graphite annually. BloombergNEF projects that a quadruple increase in graphite demand by 2030, and an astonishing 25-fold increase by 2040 compared to 2021, indicating an impending shortage in the natural flake graphite market as early as 2022, as illustrated in Figure 6c.[22,23]

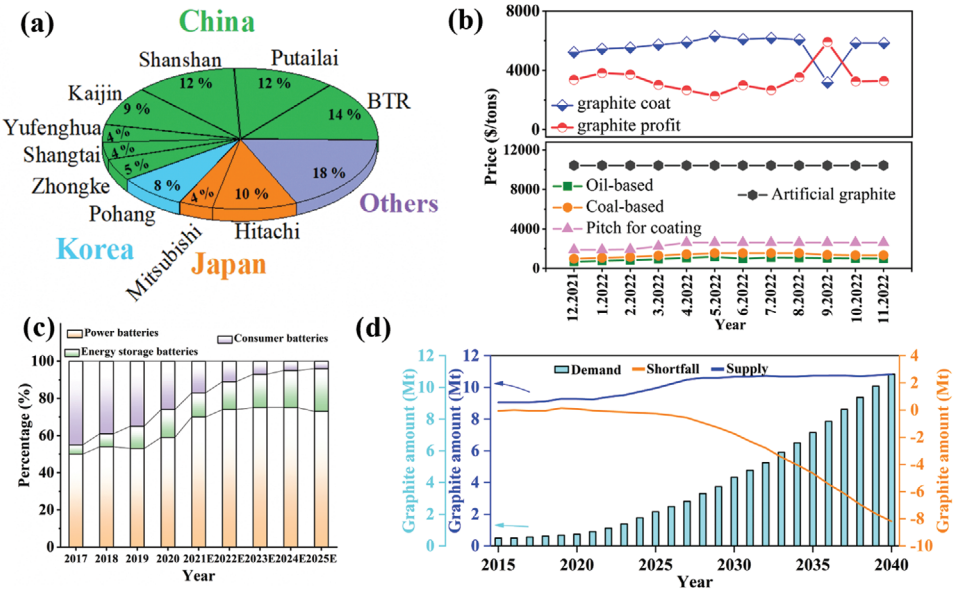

Figure 6. a) Global graphite material market landscape in 2020. b) The price trend of the raw material of graphite anode material (petroleum-based, coal-based coke and pitch for coating) and itself (Mysteel.com). c) The bar graphical growth data of market share of power batteries, consumer batteries and energy storage batteries in 2017–2020. d) Graphite shortage starting in 2022-shortage to grow to 8 Mt by 2040.[22,23]

Considering the information presented, a cumulative total of 1.6 Mt end-of-life LIBs are expected to be generated, resulting in ≈16 kt of retired power battery annually by 2030.[24] However, LIBs recycling is not yet widely established worldwide, with the current global waste recycling rate for LIBs at only 3–5%. The used recycling processes are cost-effective but outdated, lacking maturity and large-scale efficiency, and mainly focus on recovering scarce secondary resources such as lithium, nickel, and cobalt.[25–30] The Democratic Republic of the Congo is by far the largest producer of cobalt intermediates, where almost 70% of the world's cobalt mining takes place, but is linked with armed conflict, blatant human rights violations and harmful environmental practices. Indonesia holds most of the world's nickel ore reserves. Australia and Chile together contribute to 77% of global lithium production, while China produces 65% of world's graphite. The prices of these most vital components have fluctuated substantially in recent years.[23] Depending on the battery type and application, the graphite content in LIBs can be ≈10–20 times higher than that of the best-known crucial lithium.[31] As shown in **Figure 7**, graphite material typically occupies ≈10–28 wt% of the composition in various cylindrical (18650, 21700 and 4680), prismatic and pouch configurations employing different metal oxide cathode types. This accounts for ≈8–10% of the overall battery manufacturing cost in LIBs.[32] Furthermore, the European Commission's report titled "Raw Materials of Life and Death for the EU" designates graphite as one of the fourteen critical raw materials. Given the limited availability of mine resources and the high cost of purification, the effective reclamation of graphite, a key component in anodes, has become both economically attractive and environmentally urgent. However, spent graphite lacks a clearly defined path for large-scale and economically viable recycling.

Recycling of used LIB streams provides resilience against vulnerable supply risks in the "circular economy" of LIB, which also simultaneously preserves a clean environment, as one 20 g cell phone battery can pollute 1 km^2 of land for up to 50 years,[33] not only directly threatening ecosystems organisms on trophic levels, but causing catastrophic fires incidents as well. As the German Federation of Steel Recyclers claimed that 80–90% of reported fires breaking out in associated sites in 2019 in Germany were involved by highly explosive and flammable lithium batteries.[34] Notwithstanding many research groups urgently calling for the repurposing of graphite from expired LIBs, the dominant bottleneck is currently the simplicity of the approach and the economic profitability.

2. Failure of Graphite Anode Material

Li-ion batteries depending on the system and configuration have a certain probability of failure during use or storage, which is commonly caused by various reasons. For instance, particle fragmentation due to uneven stress caused by inconsistent local Li^+ de-intercalation rate, fragmentation and pulverization of silicon anode material due to volume expansion and contraction upon charging and discharging. Continuous decomposition or degradation of the essential components or additives of the electrolyte due to humidity and temperature, leads to irreversible reaction with the electrode and increases the cell impedance. N/P design (cell balance: the ratio of the capacity of negative electrode to the capacity of positive electrode) is often either too low, resulting in lithium precipitation; or too large leading to shallow discharging of the negative electrode and deep charging of the positive electrode, inducing an elevated oxidation state to lure safety hazards. There are numerous other abuse conditions such as overcharge/overdischarge, abnormal voltage, low/high temperature operation, external/internal shorting, deformation etc. Often different failure reasons are superimposed to finally lead to battery failure or even thermal runaway. For example, faster

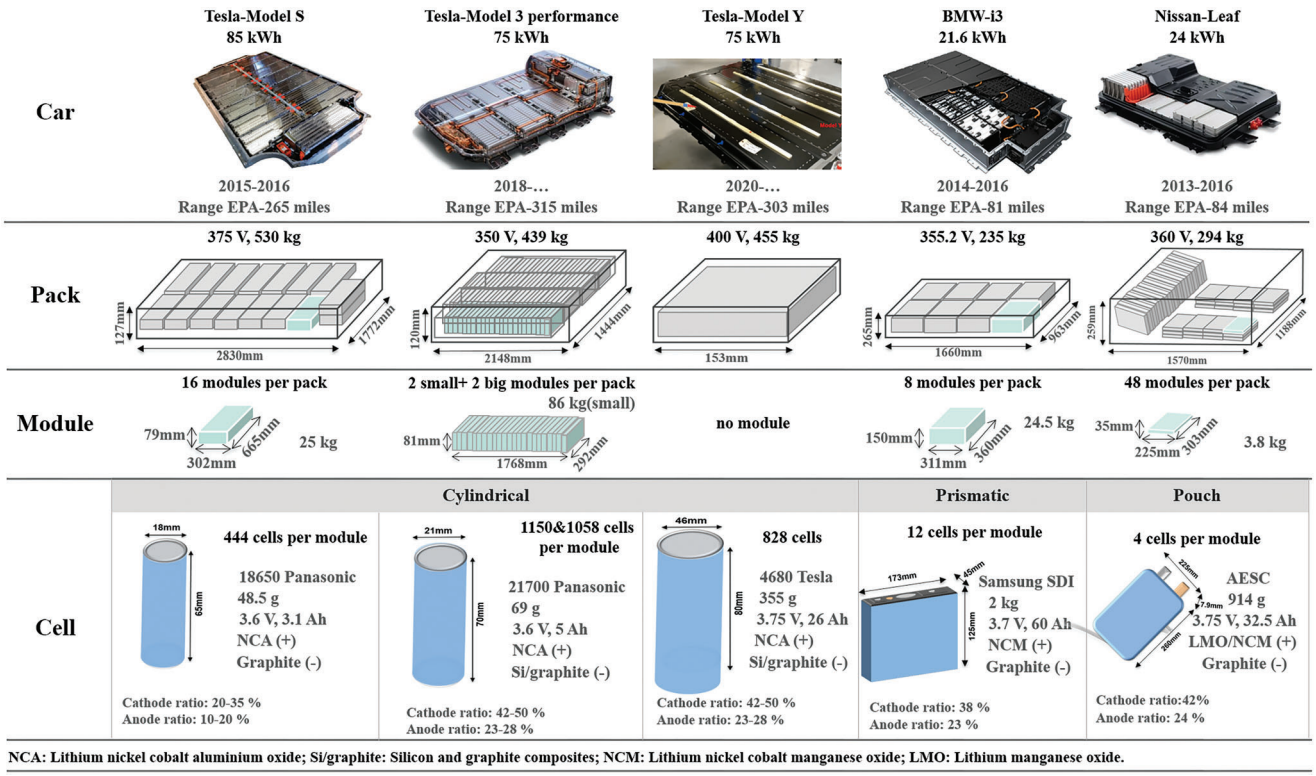

Figure 7. Examples of five different battery packs and modules (cylindrical 18650, 21700, and 4680 cell, prismatic and pouch) currently used in electric vehicles (The pictures of car row are from analiticaderetail.com, http://redgreenandblue.org/2018/07/09/battery-pack-dance-off-tesla-model-3-versus-chevy-bolt/, http://www.asianev.com/news/show-11164.html, https://www.torqeedo.com/de/technik-und-umwelt/battery-technology.html and http://m.cbea.com/qyjs/201712/982691.html. All the data from EVcompare.io and reference,[32] Reproduced (Adapted) with permission.[32] Copyright@2019, Springer Nature Limited.

charging and discharging may manifest as a large polarization at the beginning, a continued formation of lithium metal precipitation at the intermediate stage will lead to growth of lithium dendrites, piercing the separator and internal short circuiting. In the final stage, due to a rapid heat generation, the internal temperature will rapidly collect and spontaneously rise, accompanied by a series of self-sustained cascading exothermic reactions with the toxic electrolyte and carcinogenic electrolyte additives and lithium dendrites, which will eventually trigger thermal runaway and spread one to neighboring cells, emit a mixture of noxious gases (HF, POF_3, NO_x, SO_x, CO_x, HCl, HCN), particles and chemicals released from LIBs.[35] This sections' emphasis is placed on the failure behavioral characteristics of the graphite anode. The failure mechanisms associated with the graphite anode materials during cycling are mainly related to the decomposition of the SEI film, the formation of lithium dendrites, the continuous change in volume leading to pulverization and shedding of active material particles, the decrease of graphitization, the contact loss, inhomogeneity of electrolyte wetting and corrosion of the current collector.

2.1. SEI Generation and Growth

In 1979, Peled first coined a pioneering solid electrolyte interphase (SEI) model, which illustrated the deposition-dissolution mechanism of alkali and alkaline earth metals in the SEI non-aqueous battery systems.[36] One of the primary causes of the cathode degradation in LIBs is considered to be the change in the electrode/electrolyte interface. The composition of the SEI is thermodynamically unstable, and both its composition and thickness vary. Its composition is closely related to the composition of the electrolyte. The fluorinated electrolyte salt such as $LiPF_6$, $LiBF_4$, $LiAsF_6$ (thermal stability: $LiASF_6$ > $LiBF_4$ > $LiPF_6$, the fusion temperature is 320 °C for $LiBF_4$ and 100 °C for $LiPF_6$) and other fluorine-containing lithium salts lead to the formation of LiF as the SEI component.[37] The decomposition of solvents such as ethylene carbonate (EC), propylene carbonate (PC), dimethyl carbonate (DMC), ethyl methyl carbonate (EMC), diethyl carbonate (DEC), fluorinated ethylene carbonate (FEC), vinylidene carbonate (VC) and other carbonate organic solvents leads to the formation of lithium carbonate (Li_2CO_3) and alkyl Li_2CO_3.[38] The harsh conditions of powered LIBs can lead to a thicker SEI precipitation, and a damaged SEI can exacerbate electrolyte loss resulting in blocking Li^+ conducting channels, thereby deteriorating the battery performance. Thermal, chemical and mechanical failures are the main failure modes encountered by the SEI. Zhang et al. investigated the influence of current densities (0.2 C, 1 C and 10 C) on graphite anode degradation in $LiFePO_4$||graphite three-electrode pouch cell, and the results demonstrated that large current densities lead to inhomogeneous morphology of the passivated SEI layer, intensified electrolyte and lithium ion

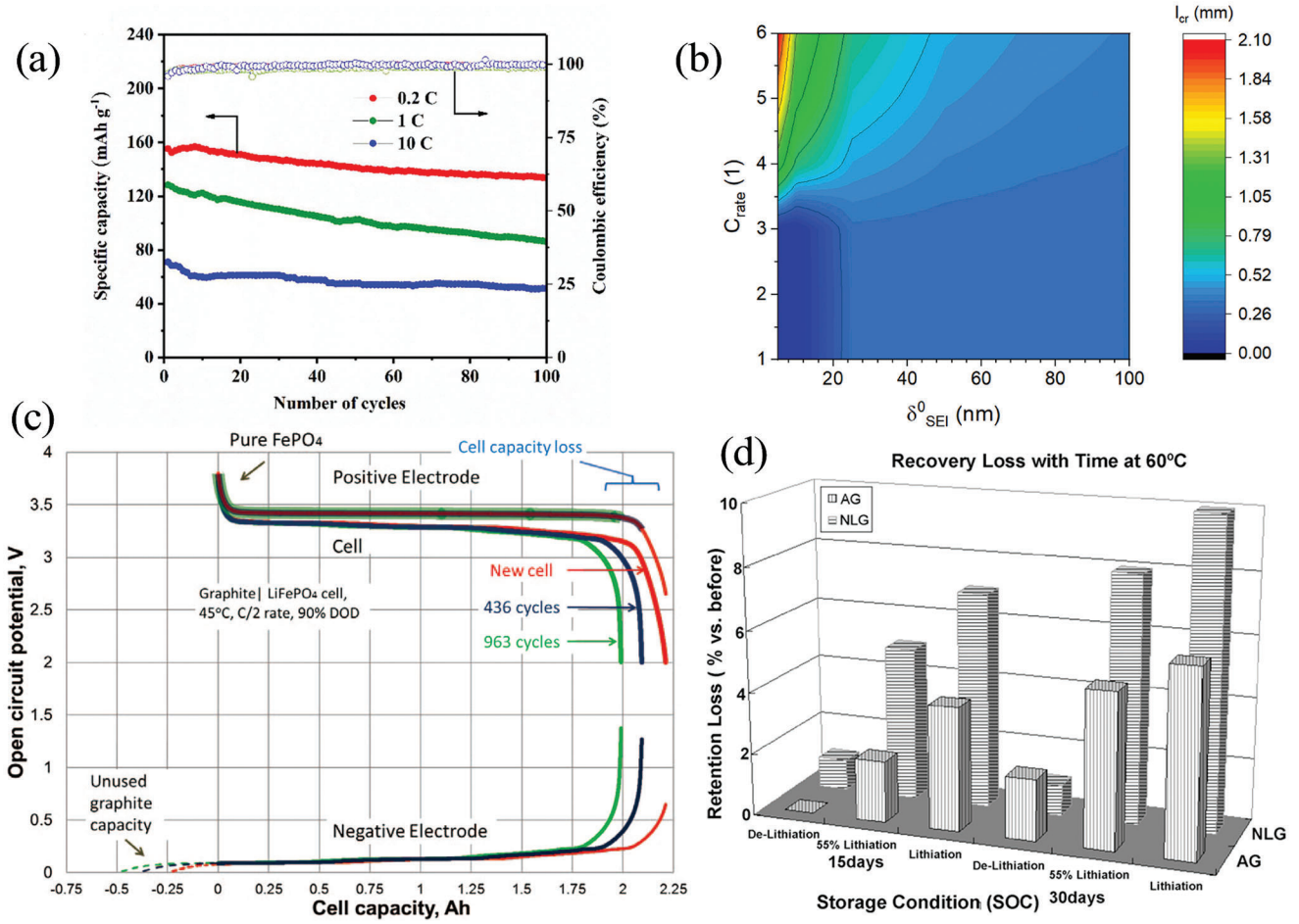

Figure 8. a) The cycling performance of the $LiFePO_4$||graphite full cell from 2 to 3.65 V.Reproduced (Adapted) with permission.[39] Copyright@2019, ECS. b) Crack length contour map over different C-rate and initial SEI thickness (I_{cr}-crack length; σ^0_{SEI}-SEI thickness). Reproduced (Adapted) with permission.[40] Copyright@2020, Elsevier. c) Plots of voltage versus capacity at different number of cycles for the data calculated using the model. The lowermost three curves represent the negative electrode potential at different cycles, and the uppermost curves, which overlay one another for most of the voltage range, depict the positive electrode potential. The middle three curves correspond to the cell potential. Reproduced (Adapted) with permission.[41] Copyright@2012, IOP Publishing. d) Recovery loss of storage cells with state of charge (SOC) and storage time (AG-Artificial graphite, NLG-Natural-like graphite). Reproduced (Adapted) with permission.[44] Copyright@2007, Elservier.

consumption, and lithium dendrite growth, which ultimately leads to capacity degradation (**Figure** 8a).[39] Sarkar et al. implemented the plating-related stress field one-step model to calculate the critical energy release rate for film cracking of NMC||graphite. The results indicate the tendency of a thin SEI to fracture at higher charging rates (Figure 8b).[40] Deshpande et al. also investigated irreversible capacity loss in $LiFePO_4$||graphite batteries, and attributed the irreversible capacity loss to diffusion-induced stressesthat lead to macroscopic ion cracking on the electrode surface, and the formation of an uncovered graphite surface exposed to the electrolyte. This further resulted in the formation SEI and/or particle isolation from the electronic network, leading to impedance growth, loss of reversible lithium ions, and capacity decay (Figure 8c).[41] Takahashi et al. have further thoroughly investigated the stress generation of the graphite at the particle scale by incorporating a mathematical stress modeling. The results showed that cracking is not likely during delithiation at 30 C at 25 °C, but clear crackings are found at rate 10 C at −10 °C attributed to a diffusion coefficient that is approximately an order of magnitude lower than that at 25 °C.[42] Xu et al. proposed that optimizing the N/P ratio in $Li[Ni_{0.8}Mn_{0.1}Co_{0.1}]O_2$||graphite cell could minimize the initial lithium inventory loss, the initial irreversible capacity and the SEI sustained growth.[43] Kwak et al. conducted surface analysis of the negative electrode material after disassembling the cells and storing them at 60 °C for different periods of time, and the results indicated that the irreversible lithium loss resulted from the thickening of the negative electrode material's own SEI as the storage time increased (Figure 8d).[44]

2.2. Lithium Dendrites Generation

Graphite anodes have a low lithium insertion potential (≈0.1 V), thus posing the risks that under certain conditions such as overcharging, large rate charging/discharging, low temperature

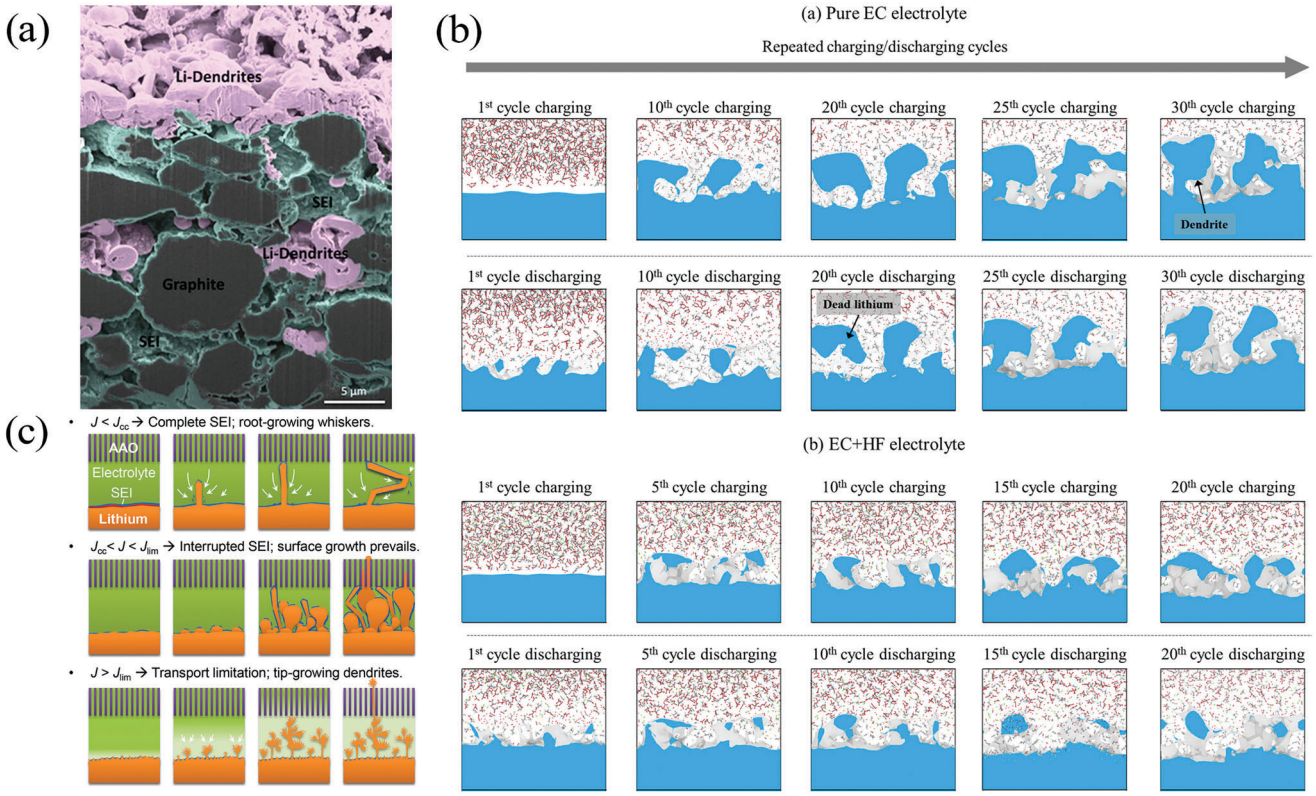

Figure 9. a) Pseudo color image of the cross section of an aged graphite electrode after osmium tetroxide staining. Reproduced (Adapted) with permission.[46] Copyright@2014, Elsevier. b) Growth of dead lithium and dendrite in pure EC electrolyte and suppressed growth of dead lithium and dendrite in EC + HF electrolyte during repeated charging/discharging cycles. Reproduced (Adapted) with permission.[47] Copyright@2022, Springer Nature. c) Schematic illustrations of the mechanism for lithium dendrites. Reproduced (Adapted) with permission.[50] Copyright@2018, Elsevier.

operation etc., the negative electrode lithium insertion potential drops below 0 V, and metallic lithium dendrites will be formed at the electrode surface. The dendrites are prone to pierce the separator, causing a short circuit inside the battery. This situation may cause destructive failure of the battery, and the dendrites are difficult to be detected before the occurrence of a short circuiting in the battery.

The growth process of lithium dendrites can be observed in situ through transparent cells constructed by quartz glass. Rong et al. revealed the in situ observation of lithium dendrite growth relying on SEM technique. The findings demonstrate that the growth rate and mechanism of lithium dendrites are strongly influenced by the additives in the ether-based electrolyte.[45] In order to determine the location of dendrite growth, Zier et al. proposed to map the electrode electron microscopy by staining the electrode structure with osmium tetroxide (OsO_4) staining. Using the high affinity of the lithium metal to react with the OsO_4, it is possible to locate even very small lithium deposits on graphite electrodes (**Figure 9a**).[46] Lee et al. performed a series of reactive molecular dynamics simulations that allow real-time interfacial visualization of the dynamic growth of dead lithium and dendrites during repeated charging (Figure 9b).[47] Song et al. proposed operando neutron imaging to reveal the dynamic distribution of lithium flowing from the anode to the cathode during charging due to an internal short circuiting caused by lithium dendrite growth.[48] Bai et al. proposed a quantitative safety boundary conditions called "Sand's capacity" allowing to visualize the growth of dendritic lithium in a glass capillary cell. The results show that there are two different mechanisms of a lithium growth in liquid electrolyte depending on the current and capacity. Namely, reaction-limited mossy lithium mainly grows from the roots and cannot penetrate hard ceramic nanopores in a sandwich cell below Sand's capacity, but transport-limited dendritic lithium grows at the tips and can easily cross the separator to short the cell above Sand's capacity.[49] Further, Bai et al. and parallel to Bazant et al. constructed two types of symmetrical lithium batteries to investigate the safety boundaries for the given applied current densities and area capacity. They identified two critical current densities, revealed three growth modes of lithium dendrites, and evaluated the risks associated with these modes. Furthermore, they proposed a set of practical safety bounds as well as tactics to optimize the design of rechargeable metal cells (Figure 9c).[50] Shen et al. proposed in situ strong electrochemical atomic force microscopy study of initial Li deposition in EC and FEC electrolytes on graphite anodes. These results indicate that the SEI formed by the FEC-based electrolyte can inhibit the growth of Li-dendrites. The FEC-based electrolyte induces the formation of LiF-rich SEI membranes that are stiffer and denser than those formed in the EC-based electrolyte.[51] Luo et al. demonstrated a proof-of-concept graphite anode containing a polymer coating that effectively mitigates the formation of Li dendrites under harsh lithiation conditions. The

results show that Li dendritic crystals ranging in size from tens of nanometers to microns readily undergo fast lithiation under 20% over-lithiation at 0.2 C or at a rate of 10 C on a granular graphite electrode.[52] Wang et al. investigated the electrochemical performance of pouch $LiFePO_4$ with a 10-year calendar life at different temperatures of −10 °C and different current densities. The thermal safety of the cells was investigated using accelerated calorimetry after cycling at different conditions and aging at high temperatures to evaluate the thermal abuse behavior of the cells. The results indicate that the main reasons for the degradation of electrochemical performance during low temperature cycling are the increase in internal resistance and the formation of non-electrochemically active lithium dendrites on the anode surface.[53] Pan et al. also performed density functional theory (DFT) simulation and continuous charge/discharge experiments of $LiFePO_4$/graphite full cells to explain the mechanism and phenomenon of dendrite suppression.[54] Cheng et al. claimed that nanodiamond is used as an electrolyte additive to co-deposit with lithium ions and produce dendrite free lithium deposits. First principles calculations indicate that lithium prefers to adsorb onto nanodiamond surfaces with low diffusion energy barriers, leading to uniformly deposited lithium arrays. Uniform lithium deposition morphology results in enhanced electrochemical cycling performance.[55]

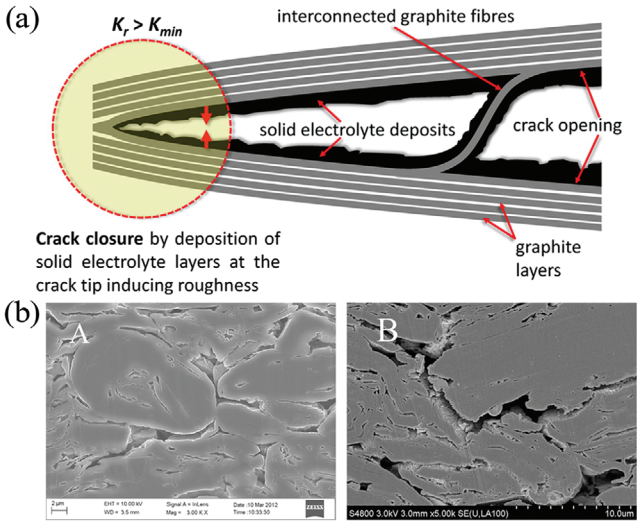

Figure 10. a) A schematic showing the occurrence of mechanisms responsible for possible reduction in graphite crack growth.Reproduced (Adapted) with permission.[56] Copyright@2011, Elsevier. b) Cross-section of graphite anode before cycling and after 100 charge/discharge cycling at 45 ± 1 °C. Reproduced (Adapted) with permission.[57] Copyright@2013, Elsevier.

2.3. Volume Expansion During Cycling

Negative electrode materials are susceptible to material cracking and rupture, i.e., microcracking of the material, during iterative lithiation/delithiation process. In general, with the extended use of the battery, micron-sized particles, due to the internal stresses of ion insertion may crack. The initial cracking is usually found on the surface of the active material particles by SEM, and as the lithium ions are repeatedly intercalated and deintercalated, the cracking continues to extend. The cracked particles not only form a new active surface on which SEI films are produced, but also lead to damaged disordered graphite structures. Bhattacharya et al. observed the formation and extension of cracks in electrochemically cycled graphite electrodes in LIBs by transmission electron microscopy and found that the deposition of the SEI layer at the crack tip may have reduced the effective cyclic stress intensity factor, thus decreasing the crack growth rate (**Figure 10a**).[56] Liu et al. demonstrated by using micro-Raman mapping at a lateral resolution of 2 µm that stresses are generated and accumulate mainly in the early cycling process, which leads not only to large expansion of the anode thickness, but also to cracking and even degradation of the graphite particles (Figure 10b).[57] Lin et al. investigated the structural degradation of graphite anodes with different number of cycles and charging rates by focused ion beam and SEM. Cracks appeared in most of the graphite particles near the lithium insertion surface, which may originate from the stresses generated during the lithiation and de-lithiation cycles.[58] Wang et al. developed a coupled electrochemical and mechanical model at the fine scale to evaluate the strain and stress in the anode particles during the charging process. The results reveal that the tuning of the following parameters such lower charging rate, spacing factor, electrode thickness, and diffusion coefficient can reduce the stress in the anode particles.[59] Montin et al. presented a 3D coupled diffusion mechanical numerical model that simultaneously accounts for crack nucleation through (i) a random particle generator and (ii) a stochastic description of material properties implemented within the lattice. Irregularly shaped active particles may suffer up to 60% more mechanical damage than other equivalent spherical particles, while material defects may lead to up to 110% more damage increment.[60]

2.4. Contact Loss

Contact loss leads to higher impedance. Vetter et al. proposed that the inter-electrode contact losses, i.e., mechanical disintegration, occurs between (1) carbon particles, (2) the collector and carbon particles, (3) binder, (4) binder and carbon particles, and (5) binder and collector.[61] Chen et al. prepared a new type of copper foil collector by asynchronous rolling and surface morphology modification, which improved the interfacial adhesion between the collector and the active material (surface roughness R_a = 1.8 um, significantly higher than that of conventional electrodeposited copper foil R_a = 0.22 µm) (**Figure 11a**).[62] Huersker et al. investigated the mechanical integrity of Na-carboxymethylcellulose (CMC), polyvinylidene fluoride (PVdF) and CMC/styrene butadiene rubber (SBR) blends for graphite electrodes by in situ electrochemical dilution.[63] They found that the maximum and minimum thicknesses of the PVdF-based electrodes remained constant during the anion intercalation/de-intercalation, while the CMC-based electrodes showed a thickness increase in the first cycle and a decrease after reaching a maximum electrode thickness. Landesfeind et al. compared two aqueous (CMC/SBR and alginate) and three NMP-based (PVdF, Kynar, Kureha and Solef) binder systems and analyzed their centrifugal permeability according to Nyquist plots (Figure 11b).[64]

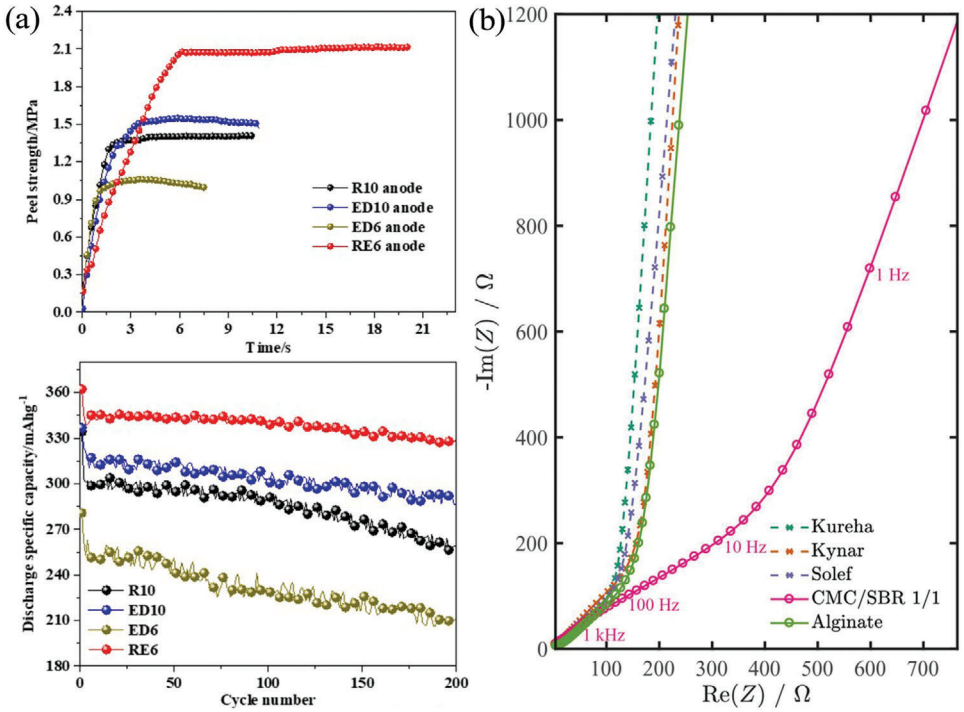

Figure 11. a) Peel strength of different anodes and cycle performance. Reproduced (Adapted) with permission.[62] Copyright@2021, Elsevier. b) Nyquist plots of symmetric cells using graphite electrodes without conductive carbon additive and with 6 wt% water based (solid lines, circles) and NMP based (dashed lines, crosses) binders. Reproduced (Adapted) with permission.[64] Copyright@2018, ECS.

Fabian et al. systematically described the effect of the amount of inactive material binder on the performance of graphite anode. They demonstrated that high binder contents of 8 wt% or more show significant cycle life improvements over binder contents of 4 wt% or less.[65] Kupper et al. identified dry-out as the main cause of contact loss between the active material particles and the electrolyte by modelling mechanical aging.[66]

2.5. Non-Uniform Electrolyte Wetting

The wettability of the electrolyte to the electrodes is an important factor that must be considered in the evolvement of high-performance LIBs. Uneven wetting causes an uneven distribution of current density and unstable SEI film formation. Incomplete wetting of the electrodes also affects battery performance and can cause a precipitation of lithium metal from the negative electrode, thus posing a serious safety hazard. Jeon investigated the kinetic properties of electrolyte diffusion in a 2D lithium-ion electrode model using a multi-phase lattice Boltzmann method. It was documented that an increase in the lapping ratio of the electrode leads to a significant decrease in electrode wettability, especially at high solid densities, where the electrolyte wettability in the vertical electrode direction is very small and the electrolyte is mainly concentrated on the electrode surface and the separator. At the same lamination ratio, the negative electrode is less wettable than the positive electrode due to the more enhanced deformation of the particles during lamination (**Figure 12a**).[67] Davoodabadi et al. proposed the in-plane imbibition method and investigated in detail the effects of electrolyte salt concentration and electrolyte solvent in conjunction with theoretical analysis. The wetting rate of the electrolyte can be increased. Furthermore, for the electrolytes tested in this study, the adsorption of electrolyte into un-calendered graphite anode was much faster than that of the uncalendered NMC532 cathode. The results reveal that an increase in salt concentration adversely affects the wetting rate of the electrolyte and that switching from the EC-DEC system to the EC-EMC system increases the wetting rate of the electrolyte (Figure 12b).[68] Ma et al. claimed fluoroethers instead of conventional carbonate-based electrolytes for graphite anodes and showed that they have a tenfold climb in energy density and are thermally more stable than carbonate electrolytes (operating up to 60 °C) by producing a robust solvent-derived solid electrolyte interface (Figure 12c).[69]

3. Recycling Strategies for Waste Graphite

In accordance with the principles of circular economy aimed at reintroducing end-of-life materials into the economic cycle, Ciez et al. reported the greenhouse gas (GHG) emissions resulting from battery manufacturing, utilizing CO_2 equivalent (CO_2e) values and warming potentials for twenty years (**Figure 13a**).[26] Approximate 6–11 kg CO_2e emissions per kg of cell were emitted during the manufacturing of NCA, NCM and LFP cylindrical and pouch cell batteries, of which 0.33 kg CO_2e per kg cell is due to transportation. To further investigate GHG of the graphite recycling, Rey et al. compared exemplarily the contribution of nine graphite recycling processes to environmental indicators such as global warming, ozone layer depletion potential, ecotoxicity, eutrophication or acidification by quantifying them.[70] Seven of

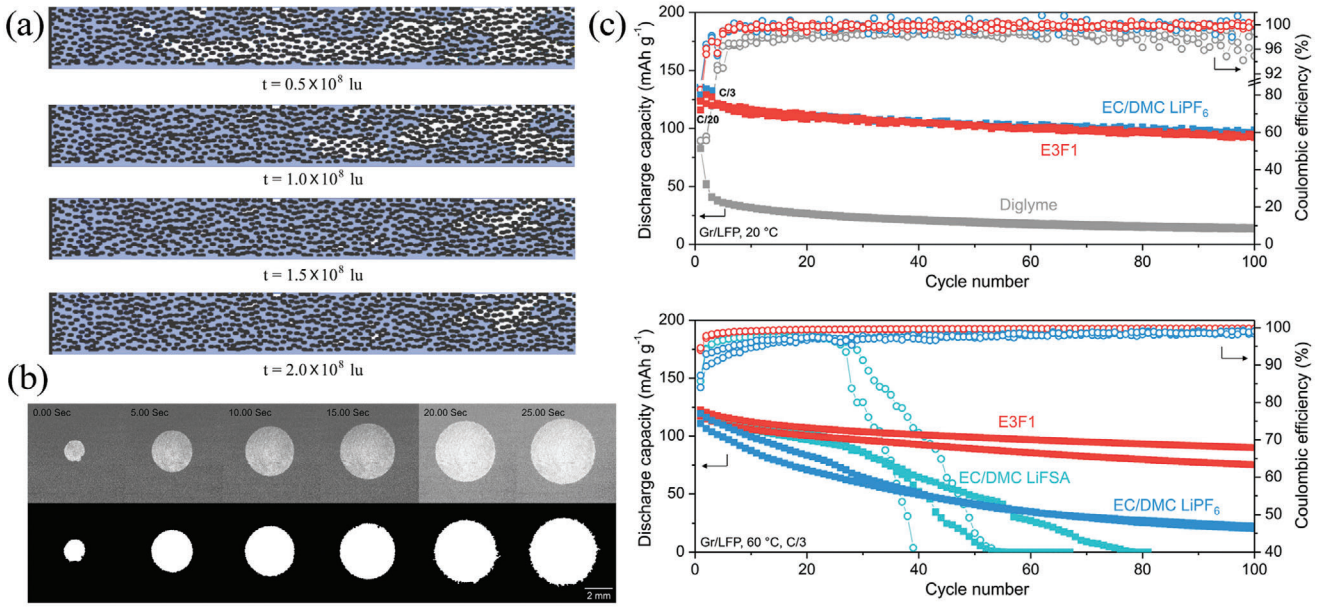

Figure 12. a) Invasion of liquid electrolyte through the pore in the separator and anode, snapshots of liquid electrolyte distribution. Reproduced (Adapted) with permission.[67] Copyright@2019, Elsevier. b) Snapshots of the imbibition process of the electrolyte #5 into the A12 electrode obtained by an optical camera from the bottom view, showing that the wetted region is radially symmetrical around the center. Reproduced (Adapted) with permission.[68] Copyright@2019, Elsevier. c) Galvanostatic cycling of graphite/$LiFePO_4$ using 1 M LiFSA in E3F1 (E3F1), 1 M LiFSA in diglyme (diglyme) and 1 M $LiPF_6$ in EC/DMC (EC/DMC $LiPF_6$). 1 M LiFSA in EC/DMC (EC/DMC LiFSA). Reproduced (Adapted) with permission.[69] Copyright@2022, RSC Publishing.

these works focused on recovered graphite and its application to secondary batteries, and two of them used graphite as a virgin material to synthesize value-added materials such as graphene oxide. The authors prepared the ReCiPe 2016 Midpoint method and combined it with the global warming potential (GWP) (kg-CO_2 equiv.) to perform a life cycle assessment (LCA) for the recycling of discarded graphite (Figure 13b). The life cycle interpretation study was conducted using OpenLCA software and Ecoinvent 3.7 Dataset. A scale up of 100 kg of waste graphite, where values ranged from 0.53 to 9.76 kg CO_2e per 1 kg graphite, was conducted and sensitivity analysis was performed to explore environmentally friendly application options. The results demonstrated that energy consumption and waste acid generation were the main environmental drivers. By limiting the amount of H_2SO_4 to a quarter, the impact could be shrunk by 20–73% (Figure 13c). Lima et al estimated that the value obtained from recycling LIBs in 2018 would be 20 \$ kWh^{-1} over a period of ten to twenty years. For an energy storage system, recycling includes decommissioning costs of ≈16 \$ kWh^{-1}.[71a] To meet Europe's annual battery production target of 300 GWh, ≈270 kt of battery-grade graphite are required. Moreover, EverBatt has been developed by Argonne National Laboratory as a model to calculate a closed-loop battery recycling cost and environmental impacts.[71b] Hence, it is urgently required to restore graphite from used LIBs in terms of environmental, humanitarian, and economic implications.

After the batteries are completely discharged, the discarded graphite material is obtained by manual disassembly, machine crushing, and sieving. Throughout the process, some undesirable metal impurities (Li, Al, Co, Ni, etc.), organic electrolytes and binders are inevitably entrapped in the graphite, affecting its subsequent material recovery efficiency. Large and multifaceted collaborations between academia and industry are essential to enable the understanding of the practical needs for diversification of the recycling technologies and material properties for industrialization.

3.1. Industrial Strategies

EV battery packs recovered from automotive applications must be disassembled to module level at least, and then the battery management systems and functional components have to be removed to obtain single cells.[32] To prevent short-circuiting and dangerous explosion risk during cells disassembly process, the industry now commonly utilizes used batteries immersed in a concentration of 5–15 g L^{-1} salt solution (commonly a sodium salt NaCl or Na_2SO_4) as a conductive solution to discharge in the pretreatment step, and left for about a week. The technique allows processing used batteries in batches, but also tends to corrode the outside of the battery, resulting in a massive amount of liquid electrolyte inside to flow out the outside. Some small-scale enterprises connect the positive and negative terminals of retired batteries to a load-bearing circuit discharge equipment for physically self-discharge for ≈8 hours. However, the efficiency of this route does not match the end-of-life rate of used batteries. Currently, some progress has been made toward deactivating used batteries using low-temperature treatment by a few high-end manufacturers. Two such recyclers are Umicore and Toxco, which employ cutting-edge technique, namely a liquid nitrogen to pretreat exhausted batteries at low-temperature −200 °C to deactivate them, and then crushed safely. Such deactivation method has

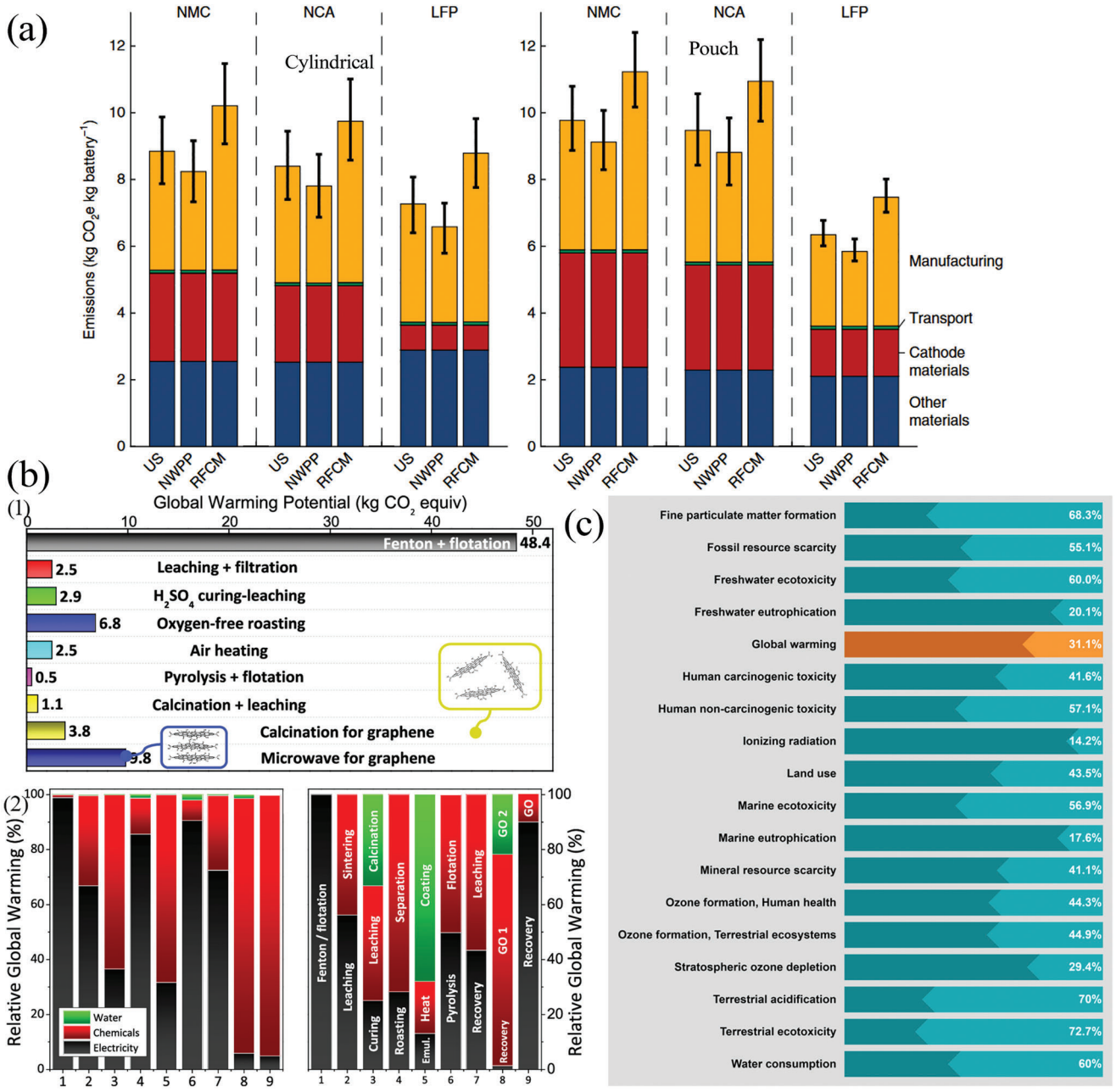

Figure 13. a) Median CO_2e emissions per kg of cell during the manufacturing of NMC, NCA, and LFP cylindrical and pouch cell batteries using US, NWPP, and RFCM average grid emissions data. Error bars represent 95% confidence intervals. Reproduced (Adapted) with permission.[26] Copyright@2019, Springer Nature. b) Global warming potential of graphite recycling processes from spent lithium-ion batteries: (1) GWP values in kg.CO_2 equiv. emissions for 1 kg of recovered graphite from spent LIBs, (2) Relative CO_2 emissions from electricity, chemicals, and water used in each graphite recovery process (left); relative CO_2 contribution from each step during graphite recycling (right). c) Sensitivity analysis of graphite recycling based on a modified H_2SO_4 curing–leaching method with a graphite:sulfuric acid ratio of 4:1 instead of the original 1:1. Reproduced (Adapted) with permission.[70] Copyright@2021, American Chemical Society.

the advantage that, in principle, is efficient and environmentally desirable, but places relatively high demands on the equipment. After crushing, the retired batteries are sieved to remove the outer packaging, and screening out black powders which are unprocessed anode and cathode. **Table** 2 presents a study of global retired LIBs recycling market research. Most of the world's leading recycling manufacturers dominantly use both the more established hydrometallurgical and pyrometallurgical assisted recycling technologies to require access to strategic elements and critical black powder for key components. Remarkably, the reclamation of valuable metal ions such as cobalt, nickel, manganese, and lithium from waste cathode materials has become a top priority owing to potential value creation and scarcity of metal resources. State of the art recycling of

Table 2. Global retired LIBs recycling market research.[72]

	Manufacturers	Countries	Approaches	Details
First-tier (Processing capacity (spent LIBs) >3 000 t $year^{-1}$)	Umicore	Belgium	Main Pyro (high temperature)	Ni-Co alloys, Li compounds Processing capacity (spent LIBs) 7000 t $year^{-1}$ [72b]
	Brunp	China	Thermal + Mech + Hydro	Ternary precursors Processing capacity (spent LIBs) 120 000 t $year^{-1}$
	GEM	China	Mech +Pyro + Hydro	NCM and NCA ternary precursor Processing capacity (spent LIBs) 10 000 t $year^{-1}$
	Taisen Recycling	China	Hydro	Processing capacity (spent LIBs) 6000 t $year^{-1}$
	SungEel HiTech	South Korea	Mech+ Hydro	NCM precursor, Li_3PO_4 Processing capacity (spent LIBs) 8000 t $year^{-1}$
	Glencore	Norway	Hydro	Ni, Co, Cu Processing capacity (spent LIBs) 7000 t $year^{-1}$
	Accurec GmbH	Germany	Thermal+Mech+ Pyro + Hydro	Co-Mn alloys, Li compounds Processing capacity (spent LIBs) 3000 t $year^{-1}$
	Nickelhütte Aue	Germany	Thermal + Pyro + Hydro	NiCoCu-Matte Processing capacity (spent LIBs) 7000 t $year^{-1}$
Second-tier (Processing capacity (spent LIBs) <3 000 t $year^{-1}$)	Kyoei Seiko	Japan	Pyro	Ni, Co, Cu
	Dowa	Japan	Thermal + Pyro + Hydro	Ni, Co, Cu
	AEA	UK	Electrodeposition	product CoO
	Recupyl	France	Mech+ Hydro	product Li_2CO_3, $Co(OH)_3$
	SNAM	France	Thermal + Pyro + Hydro	Co, Ni, Cu
	EDI	France	Mech+Uknown	Co, Cu
	Batrec	Switzerland	Hydro	product Ni, Co, MnO
	Duesenfeld	Germany	Mech+ Hydro	Co/Li/Ni/Mn salts, graphite
	IME	Germany	Pyro + Hydro	Alloys, Ni/Co hydroxide
	GRS Batterien	Germany	Pyro	Alloys
	Redux	Germany	Thermal+Mech+ Uknown	Co/Ni salts
	Fortum	Finland	Hydro	Co/Li/Ni/Mn salts
	AkkuSer	Finland	Mech+Uknown	Co alloy, Li_2CO_3
	Northvolt	Norway	Hydro	ternary
	Mitsubishi	Japan	Pyro	product LCO
	4R Energy Corp	Japan	Laddering	Focus on laddering 10–24 kWh, 100 kWh
	Li-Cycle	Canada	Pyro + Hydro	Co/Li/Ni salts
	Retriev	United States/Canada	Mech+ Hydro	Li_2CO_3
	OnTo Technology	United States	Supercritical recovery	Recovery of formance battery
	Redwood	United States	Hydro	Co/Li/Ni salts, graphite

Mech: mechanical, Hydro: hydrometallurgy, Pyro: pyrometallurgy.

discarded LIBs involves pyrometallurgical process (smelting) and hydrometallurgical process (leaching in acid-rich aqueous solution). More common pyrometallurgical assisted route consists in melting the cathode material into iron-nickel alloy or cobalt-nickel alloy, applied for instance by Umicore in Belgium, Kyoei Seiko and Mitsubishi in Japan, GRS Batterien in Germany. While other essential components of the battery such as graphite, electrolyte, separator and conductive carbon

are burned off and are thus removed from the material cycle. This generates considerable unwanted hazardous gaseous emissions concerns and limits the recovery of other crucial components but has also a low economic effect. Nevertheless, this approach is suitable for all battery formats. Hydrometallurgy involves separating, enriching, and extracting metals by dissolving valuable metal components in solution using leaching agents, while leaching agents being acids which produce large amounts of acidic wastewater. Significant industrial players are Taisen Recycling in China, Glencore in Norway, Batrec in Switzerland, Fortum in Finland, Northvolt in Norway, Redwood in USA. To lower environmental footprints, a combination toward hydrometallurgical, pyrometallurgical, and mechanical means is the popular recycling approach for most of recyclers. For example, GEM, Brunp in China, SungEel HiTech in South Korea, Accurec GmbH and Nickelhütte Aue in Germany, etc use this approach. But there is still no standardization in the industry.

Graphite anode material recycling is not yet well underway, but with graphite resources in short supply and the urgent need to close the loop, a handful of companies are ramping up to industrialize on recycling and reusing scrapped graphite. Case in point, graphene material suppliers Graphmatech, Graphenea and battery developer Northvolt have successfully upgraded used EV batteries to graphene oxide on an industrial pilot scale.[73] The use of retired LIBs to produce graphene oxide makes the entire graphene value chain more sustainable and cost effective. Australian graphite materials company EcoGraf has formed a partnership with Korean lithium battery recycler SungEel Hitech to recover high-purity graphite material from used batteries using EcoGraf's proprietary purification process.[74] Redwood Materials in the U.S. recycles all discarded batteries from Panasonic and Tesla factories and sells much of its material back to Panasonic to manufacture new Tesla batteries.[75]

3.2. Academic Approaches

At the laboratory scale there is a small number of batteries, thus a chemical saltwater immersion or physical external resistor is basically recommended as a means of rendering end-of-life LIBs safe to discharge. Xu et al. investigated the efficiency and cleanliness of the discharge process of discarded LIBs in different salt solutions such as NaCl, KCl, $NaNO_3$, $MnSO_4$ and $MgSO_4$. $MnSO_4$ albeit having a low discharge capability, can mitigate galvanic corrosion avoiding organic leakage. But in general it is still common to use NaCl discharge to release the residual electricity from used batteries because of the high efficiency.[76] After crushing, sieving and sorting waste batteries to liberate spent anode and cathode materials, the black mass is then separated by means of selectively flotation from the strongly polar, hydrophilic positive materials and the non-polar, hydrophobic negative graphite materials by using the wettability differences between the positive and negative materials themselves, combined with trapping agents, foaming agents and adjusting agents. He et al. developed a Fenton reagent-assisted flotation process to effectively separate $LiCoO_2$ concentrates and graphite concentrates during the Fenton reaction (a solution of H_2O_2) with ferrous iron (typically $FeSO_4$ as a catalyst), macromolecule material such as PVdF was broken down into small molecules, and organic materials were oxidized into CO_2 and H_2O in the end, while 98.99% recovery of $LiCoO_2$ was achieved.[77] Zhang et al. utilized a new process combining mechanical crushing and pyrolysis-enhanced flotation in order to recover $LiCoO_2$ and graphite from waste LIBs with a recovery rate of 98% for $LiCoO_2$.[78] The graphite obtained by flotation is usually of low purity and difficult to be completely delaminated from the copper foil. Additionally, an effective and complete separation of a metallic current collector copper foil and graphite is a challenge as laboratories still mainly dismantle used batteries manually and then separate positive and negative electrodes. Cao et al. efficiently recovered graphite with 95% purity by regulating the parameters (voltage, inter-electrode distance and Na_2SO_4 electrolyte concentration) during the electrolysis process.[79] The dismantled waste graphite usually contains residual electrolyte and binder, carbon black and other impurities. The residual electrolyte typically is a mixture of lithium-containing salts, the most popular being lithium hexafluorophosphate ($LiPF_6$) dissolved in organic carbonates, which can be removed by adding additives such as EC, EMC, DMC for dissolution, while the residual binder, which is mostly PVdF, by heating in N-Methyl-2-pyrrolidone (NMP) for dissolution. In case of CMC/ SBR system, it can be dissolved by water directly. Alternatively, residual impurities can be directly pyrolyzed at 400–600 °C, and the conductive carbon black can be further removed. Afterward, the obtained discarded graphite powder can be further decontaminated and purified. The treatment of the discarded graphitic anode material can generally be divided into three feasible technical pathways in **Figure 14**,1) Acid leaching process, engaged stream to feasibly removal of metal impurities in non-purified graphite, common inorganic acids H_2SO_4,[80–86] HNO_3,[82] H_3BO_3,[87] H_3PO_4,[88] HCl.[89–92] Organic acid citric acid[93]; 2) Heat treatment, favorable to restoration of disorder lattice d-spacing among waste graphite layers destroyed due to repeated lithiation/delithiation process, reopening of Li^+ conducting channels and thus improving the specific capacity[94–97]; 3) Surface coating modification, improving the cycling strength of graphite using amorphous carbon or pyrolytic carbon from carbonized highly crosslinked polymer such as pitch,[98,99] phenolic resin,[84] sucrose, starch and glucose,[100] polyethylene glycol.[87] Hydrometallurgical recycling of graphite involves the use of inorganic and organic acids to dissolve metals/ions and should be followed by a thermal treatment to restore the graphite structure. On the other hand, hydrometallurgy solely can only remove impurities and may not effectively restore the structure of waste graphite. As a result, the combination of hydrometallurgical and thermal treatment is rapidly emerging as a preferred approach in this field. This integrated method offers the advantages of both techniques: efficient removal of metal impurities and a possible reduction in the required heat treatment temperature to below 900 °C. There are also other methods such as supercritical CO_2 extraction to extract electrolytes to eliminate residual electrolytes from graphite anodes,[101] and electrolysis,[79] microwave irradiation[102] to achieve separation of copper and graphite only.

4. Possible Applications of Recovered Graphite

The resource recycling of graphite anode holds multi-dimensional applications mainly as battery anode materials, but also graphitic carbon-related derivatives such as graphene

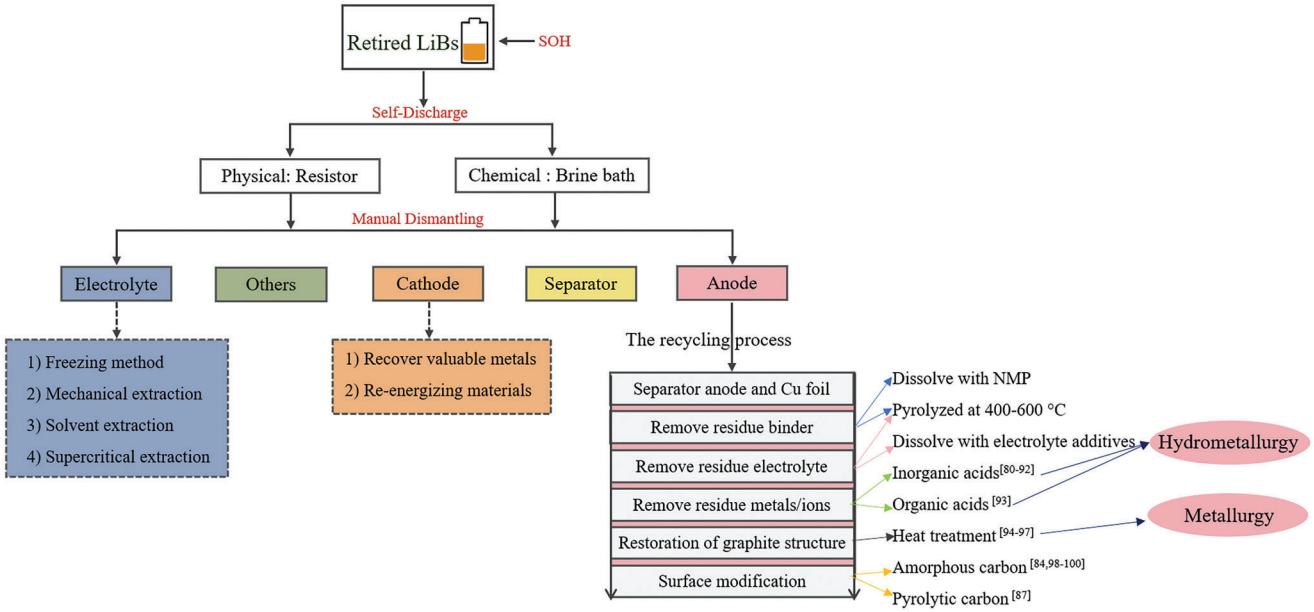

Figure 14. Entire flow chart of feasible technical routes for recycling electrolyte, cathode and anode materials of LIBs.

composite materials, nanocomposite film and catalysts, extended to supercapacitors, post-lithium-ion-batteries such as sodium/potassium ion batteries, Li-S batteries and other types as well.

4.1. Remanufacturing of New Li-Ion Batteries

A waste graphite can also find valuable use in the secondary manufacturing of LIBs. It is worth emphasizing that regenerated graphite, once well-purified, demonstrates cycling performance and stability comparable to commercially available graphite when used in battery applications (**Table 3**). This not only contributes to the sustainability of battery technology, but also offers a promising avenue for resource conservation and environmental impact reduction. This potential application of recycled graphite has been the subject of thorough examination and analysis in a recent comprehensive review[157] to which the reader is referred for further information.

4.2. Catalysts

Due to the rich functional groups and pore structure on the surface of used graphite, scrap graphite negative electrodes can also be used as catalysts after treatment. Zhao et al. recovered CuO/C catalyst from waste anode material to activate peroxynitrite to degrade various organic pollutants (Rhodamin B, Methyl orange, Tetracycline-hydrochloride and Chlortetracycline) that are hard to degrade (**Figure 15a**).[103] Liivand et al. prepared nitrogen-doped graphene oxide from expired graphite and studied the electrocatalytic activity and stability of these materials toward the oxygen reduction reaction (ORR) in alkaline 0.1 M KOH medium.[104] Nguyen et al. had investigated a carbonaceous material (ACM) prepared from waste graphite, drastically enhances the oxidation of peroxynitrite with zero-valent iron and the reduction of nitro compounds by dithiothreitol and hydrogen sulphide.[105] Wang et al. prepared reactive reduced graphene oxides from waste graphite which exhibit excellent catalytic ozone oxidation activity as reactive radicals for the removal of organic pollutants. DFT further showed that ozone molecules can spontaneously decompose into reactive oxygen species on the vacancies and edges of the graphene structure, consolidating the role of defective structures in the catalytic ozonation activity (Figure 15b).[106] Ruan et al. activated Fe-N doped carbon ORR catalysts for fuel cell applications using recycled graphite anodes, and the obtained catalysts exhibited better catalytic activity, methanol resistance, and durability (Figure 15c).[107] Chen used graphite-loaded zero-valent iron-copper bimetallic catalyst (ZVI-Cu/C) from spent LIB anodes and degraded 4-chlorophenol (4-CP) in water by reduction and non-homogeneous Fenton reaction.[108] Cao et al. effectively retreated anode waste as cathode for pollutant degradation in the electro-Fenton process by different recycling processes. The results revealed that the acid-base immersion electrode has a higher selectivity and yield of H_2O_2due to high activity of 2-oxygen electron reduction (O_2). The acid leaching electrode achieved 100% bisphenol A removal in 70 min and 87.4% chemical oxygen demand removal in 240 min, demonstrating the best degradation efficiency.[109] Zhang et al. used graphene oxide-copper composites prepared from spent LIBs to show better catalytic photodegradation performance on methylene blue, and the addition of electric field prevented the recombination of electron-hole pairs, thus generating more active free radicals, which further improved the photodegradation efficiency of graphene oxide-copper composites on methylene blue.[110] Xu et al. first proposed the direct application of waste graphite as a functional intermediate layer with enhanced polysulfide capture and catalytic performance for Li-S cells with a high discharge capacity of 968 mAh g^{-1} to obtain a low decay rate of 0.08% per cycle for 500 cycles at 1 C (Figure 15d).[111]

Table 3. Electrochemical performance of regenerated graphites (Reproduced (Adapted) with permission).[82] Copyright@2022, Elsevier.

Recycling process	Electrode information	Electrolyte	Potential range	Reversible capacity at 1st cycle	Cycling stability	Rate capacity
HCl leaching[91]	90% active material + 5% AB + 5% PVDF	1 M $LiPF_6$ in DMC:EC	0.01-2 V	591 mAh g^{-1} at 0.1 C	97.9% after 100 cycles at 0.1 C	≈172.6 mAh g^{-1} at 1 C
H_2SO_4+H_2O_2 leaching—coating[84]	94.5% active material + 1.5% AB + 4% PVDF	1 M $LiPF_6$ in DEC:EC	0.001-1.5 V	347.2 mAh g^{-1} at 0.1 C	98.76% after 50 cycles at 0.1 C	≈260 mAh g^{-1} at 2 C
H_2SO_4+H_2O_2 leaching[83]	80% active material + 10% C65 +10% PVDF	/	0.001-1.5 V	359.3 mAh g^{-1} at 0.2 C	84.63% after 100 cycles at 0.2 C	≈9 mAh g^{-1} at 5 C
Thermal treatment, CO_2-assisted[133]	90% active material + 5% SP +5% Na-CMC	1 M $LiPF_6$ in DEC:EC	0.02-1.5 V	345 mAh g^{-1} at 0.1 C	379 mAh g^{-1} after 100 cycles at 0.5 C	/
Thermal treatment (3000°C)—coating[134]	94.5% active material + 1.5% SP +1.5% CMC + 2% SBR	1 M $LiPF_6$ in DMC:EC	0.005-2.0 V	324.58 mAh g^{-1} at 0.2 C	348 mAh g^{-1} after 100 cycles at 0.5 C	≈285 mAh g^{-1} at 1 C
H_2SO_4 curing —leaching[135]	93% active material + 2% AB + 5% PVDF	1 M $LiPF_6$ in DMC:EC:EMC	0.001-2.5 V	349 mAh g^{-1} at 0.1 C	98.9% after 50 cycles at 0.1 C	≈45 mAh g^{-1} at 2 C
Microwave—CO_2[102]	80% active material + 10% AB + 10% PVDF	1 M $LiPF_6$	0.005-2.6 V	353.5 mAh g^{-1} at 0.1 C	320 mAh g^{-1} after 100 cycles at 0.5 C	≈86 mAh g^{-1} at 2 C
H_2SO_4+3000°C[96]	85% active material + 5% AB + 10% PVDF	1 M $LiPF_6$ in DMC:EC	0.01-3.5 V	351.9 mAh g^{-1} at 0.1 A/g	97.42% after 100 cycles at 0.1 A/g	/
Citric acid leaching[93]	80% active material + 10% AB + 10% PVDF	1 M $LiPF_6$ in DMC:EC:EMC	0.01-2 V	468.3 mAh g^{-1} g at 0.1 C	330 mAh g^{-1} after 80 cycles at 0.1 C	≈174 mAh g^{-1} at 2 C
Boric acid leaching[87]	80% active material + 10% SP + 10% PVDF	1 M $LiPF_6$ in DEC:EC	0.01-1.5 V	332 mAh g^{-1} at 0.1 C	325 mAh g^{-1} after 100 cycles at 0.1 C	≈140 mAh g^{-1} at 1 C
Our work H_2SO_4+HNO_3 leaching[82]	91% active material + 2.4% CB +1.5% CMC + 5% SBR+0.1% CNTs	1 M $LiPF_6$ in DEC:EC + 10% FEC	0.01-2.0 V	366.20 mAh g^{-1} at 0.1 C	363.53 mAh g^{-1} after 100 cycles at 0.5 C	≈353.27 mAh g^{-1} at 4 C

AB, acetylene black; AC, acetylene carbon black; SP, super P; C65, a type of carbon black; DMC, dimethyl carbonate; EC, ethylene carbonate; DEC, diethyl carbonate; FEC, fluoroethylene carbonate; 1 C = 372 mAh g^{-1}.

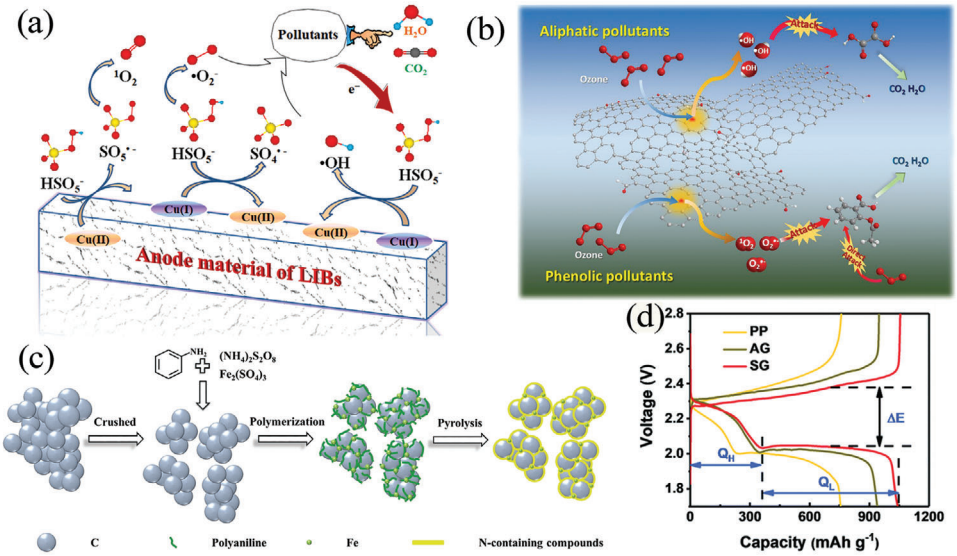

Figure 15. a) The proposed reaction mechanism of peroxymonosulfate (PMS) activation and rhodamin B degradation in anode material/PMS system. Reproduced (Adated) with permission.[103] Copyright@2021, Elsevier. b) Tailored synthesis of active reduced graphene oxides from waste graphite: structural defects and pollutant-dependent reactive radicals in aqueous organics decontamination. Reproduced (Adapted) with permission.[106] Copyright@2018, Elsevier. c) Schematic illustration of the synthetic process of catalysts. Reproduced (Adapted) with permission[107] Copyright@2021, Wiley-VCH GmbH. d) Representative charge–discharge voltage profiles of Li–S batteries with different separators (PP-polypropylene, AG-artificial graphite, SG-spent graphite) at 0.1 C. Reproduced (Adapted) with permission.[111] Copyright@2021, Royal Society of Chemistry.

4.3. Graphene Oxide & Supercapacitors

Graphene as a future revolutionary material, in recent years, has been demonstrated by researchers using graphite intercalation compounds as the initial material to obtain structurally intact graphene by directly cleaving large graphite layers makes the case for obtaining structurally intact graphite layers, but requires the use of expensive lithium metal or molten lithium hydroxide as intercalation sources. In the charge/discharge of LIBs, lithium occupies the graphite. The process of forming graphite intercalation compounds to weaken the van der Waals forces between graphite layers to facilitate exfoliation in the charging and discharging of LIBs is considered as a prefabrication step and proposed as a technical solution to prepare graphene and its derivatives by recycling anode graphite as the source material. Natarajan et al. synthesized graphitic carbon hollow spheres (CHS) and reduced graphene oxide (rGO) using scrap graphite and investigated the material for gas capture/storage. The H_2 uptake at 15 bar and 77 K was found to be 1.78 wt% for rGO and 1.22 wt% for CHS. Interestingly, the rGO obtained from the waste component showed a high CO_2 uptake of 12 and 33 wt% of CO_2 could be stored in CHS at 40 bar and 298 K. This study holds the promise of alternative/efficient gas storage materials through recycling of waste graphite (**Figure 16a**).[112] He et al. high-value utilized waste graphite from used batteries and treats it by ultrasonication through an expansion/microexplosion mechanism to produce graphene. Experimental results show that 1–4 layers of graphene can be effectively produced when charging spent LIBs with more than 50% capacity (Figure 16b).[113]

Graphene has several unique properties like a high electrical conductivity, flexibility, exceptional mechanical properties, large specific surface area (2630 $m^2\ g^{-1}$ theoretically), and an ability to store of more charge carriers and be used as an electrode material for double layer supercapacitors.[114–118] Graphene, graphene oxide or reduced graphene oxide prepared from waste graphite are a potential electrode material for supercapacitors. Natarajan et al. converted graphite from end-of-life LIBs (EoL-LIBs) into rGO and applied it in supercapacitors. The final devices exhibited a high specific capacitance of 112 F g^{-1} at a current density of 0.5 A g^{-1} with due to high surface area and mesoporous nature of the electrode material. In addition, it indicates high cycle durability of 20 000 cycles at a current density of 25 A g^{-1} (Figure 16c).[119] Natarajan et al. also prepared rGO in a simple way using spent anode graphite and Al foil after cathode lixiviation at room temperature. The electrochemical performance of the two regenerated electrodes from the spent LIB was investigated in a half-cell configuration. In addition, the constructed 3D-$MnCo_2O_4$|rGO asymmetric supercapacitor device provides an operating voltage of 1.8 V and shows a high energy density of ≈23.9 Wh kg^{-1} for 8000 cycles at 450 Wh kg^{-1}.[120] Jena et al. recovered electrode materials from spent LIBs to develop a thermally reduced graphene nanosheet-molybdenum disulfide (TRGNs-MoS_2) nanohybrid. The results showed enhanced weight capacitance values of 415 F g^{-1} with a better cycling performance with 88% capacitance maintained after 5000 charge/discharge cycles. By employing DFT, they revealed the structural and electronic properties of the TRGNs-MoS_2 hybrid structure. The excellent specific capacitance of the binary hybrid structure is underpinned by the enhanced density of electronic states close to the Fermi energy level, the lower diffusion energy barrier of the electrolytic ions, and the higher quantum capacitance of the hybrid structure (Figure 16d).[121]

4.4. Polymer Composites

Industrial polymers (polypropylene, polyethylene) and graphite materials have successively been used for the synthesis of nanocomposites with applications in modern electrochemical and microelectronic devices, such as customized conductive graphite/poly lactic acid filament which is fabricated into 3D-printed devices.[122] Pre-melt blending of expanded graphite with stearic acid and polyethylene wax, followed by powder blending and thermoforming of polyethylene particles was used to produce high thermal conductivity and electromagnetic interference shielding materials with enhanced 3D expanded graphite networks.[123] Graphite-polymer composite film with good electrical conductivity and flexibility combined with 2D VS_x (mixed phase predominated by V_5S_8) can be used for flexible wearable electronics.[124] Interlayer polymerization of chemically expanded graphite, followed by CEG in graphene——Poly(methyl methacrylate) composites can spontaneously exfoliate into monolayer and layer less graphene.[125] The design of polymer-based graphite composites based on waste graphite is also gaining attention with the concept of "The Transformation of Waste Into Wealth". Natarajan et al. synthesized composite films of polyethylene, polypropylene and graphite using recycled anode graphite and polymer separator material from used LIBs. The results showed that the specific conductance of the composite films increased by 5–6 orders of magnitude differentiate from the pure polymer films after graphite loading (**Figure 17a**).[126] Jena et al. synthesized conductive polymer composites based on waste graphite and high-density polyethylene, and the recycled graphite-based hybrid composites demonstrated high elongation and higher tensile strength compared to commercial graphite-based hybrid composites. The conductivity of HDPE-recyl-GR-5% hybrid composite was 3.81×10^{-8} S cm^{-1}, which is 10 orders of magnitude higher than high-density polyethylene (HDPE) polymers (1.17×10^{-18} S cm^{-1}) (insulator level, $< 10^{-12}$ S cm^{-1}) (Figure 17b).[127] Duan et al. fabricated conductive polyaniline/graphite nanocomposites for energy storage using waste graphite powder. The composite showed conductivity of 22.22 S cm^{-1}, a high specific capacitance up to 317 F g^{-1} and energy density 31.0 Wh kg^{-1} with 84.6% capacitance retention after 1000 cycles (Figure 17c).[128]

4.5. Na^+, K^+, and Al^{3+}-Ion Batteries

Sodium-ion (SIBs), potassium-ion (KIBs) and aluminum-ionbatteries have been identified as promising alternatives to LIBs owing to abundant and inexpensive raw materials and fear of lithium shortage. However, the storage capacity of natural graphite for Na^+ is low, with $C_{64}Na$ corresponding to a theoretical specific capacity of 35 mAh g^{-1}. The kinetics of K^+ diffusion in graphite is poor, with KC_8 having a maximum theoretical specific capacity of 278 mAh g^{-1}. Both energy density and stability

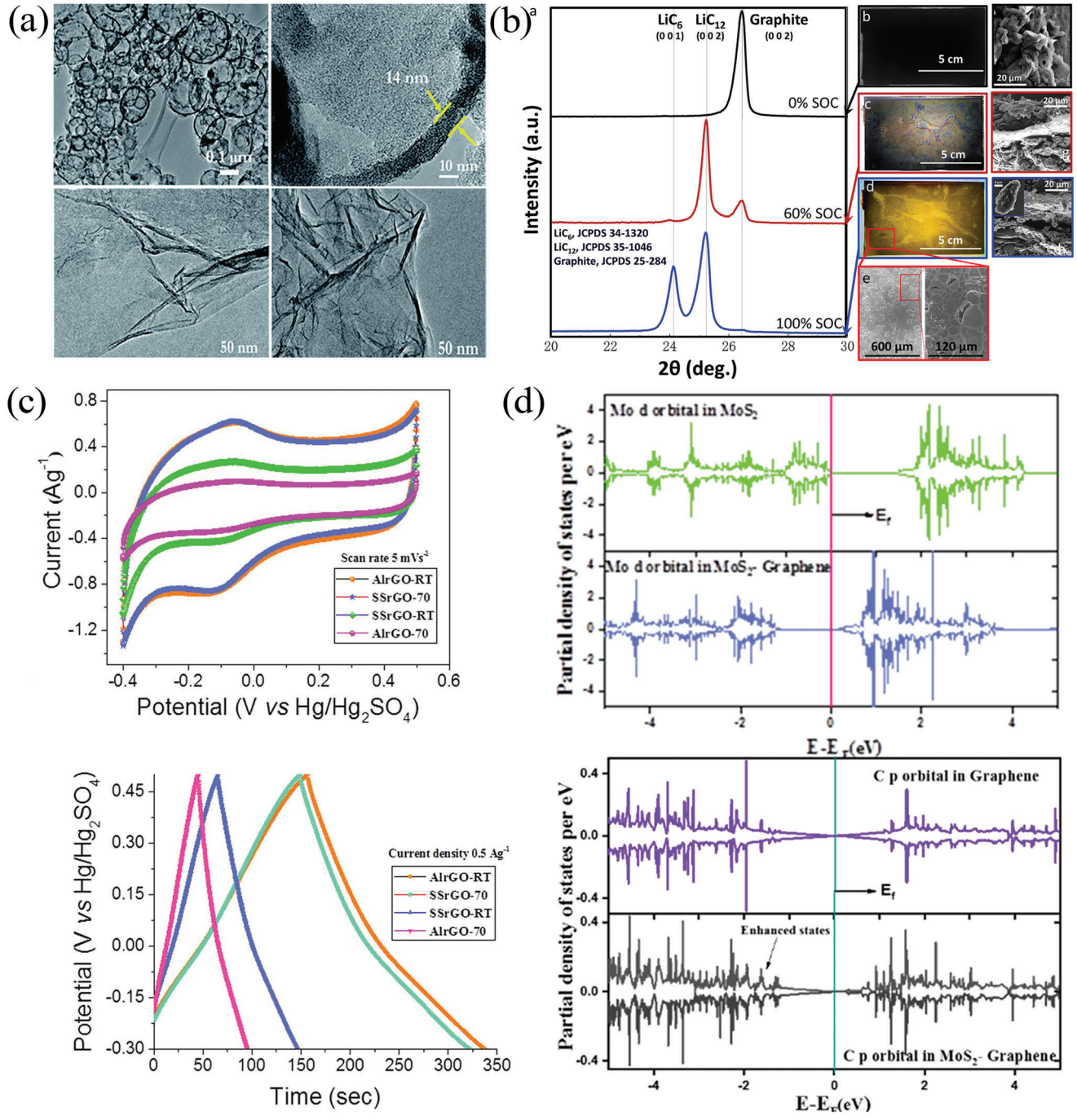

Figure 16. a) TEM images of the template-free synthesis of CHS obtained at 800 °C for 2 h (upper right and left), GO from the recovered graphite (lower left), and synthesized rGO using the outer metallic Al cases as a reducing agent at room temperature (lower right). Reproduced (Adapted) with permission.[112] Copyright@2019, Royal Society of Chemistry. b) XRD patterns and SEM images of graphite electrode with different SOC. Reproduced (Adapted) with premission.[113] Copyright@2021, Elsevier. c) Cyclic voltammetry curves and galvanostatic charging/discharging curves of four electrodes. Reproduced (Adapted) with permission.[119] Copyright@2018, Elsevier. d) Density of states per eV for the Mo d, S p, C p orbital in pristine MoS_2 and the MoS_2–graphene hybrid. Reproduced (Adapted) with permission.[121] Copyright@2022, American Chemical Society.

of the commercial graphite anode in sodium and potassium ion batteries are far from being satisfying. Sustainability wise, damaged graphite opens new windows for SIBs due to enhanced layer spacing and surface defect. In light of this issue, Liang et al. for the first-time activated graphite recovered from expired LIBs after treatment and investigated this material as potential anode for SIBs and KIBs. The visible transition phase of SIBs and the irreversible initial cyclic phase transition of KIBs were found through operando X-ray diffraction. The optimized electrode delivers improved electrochemical performance, such as 162 mAh

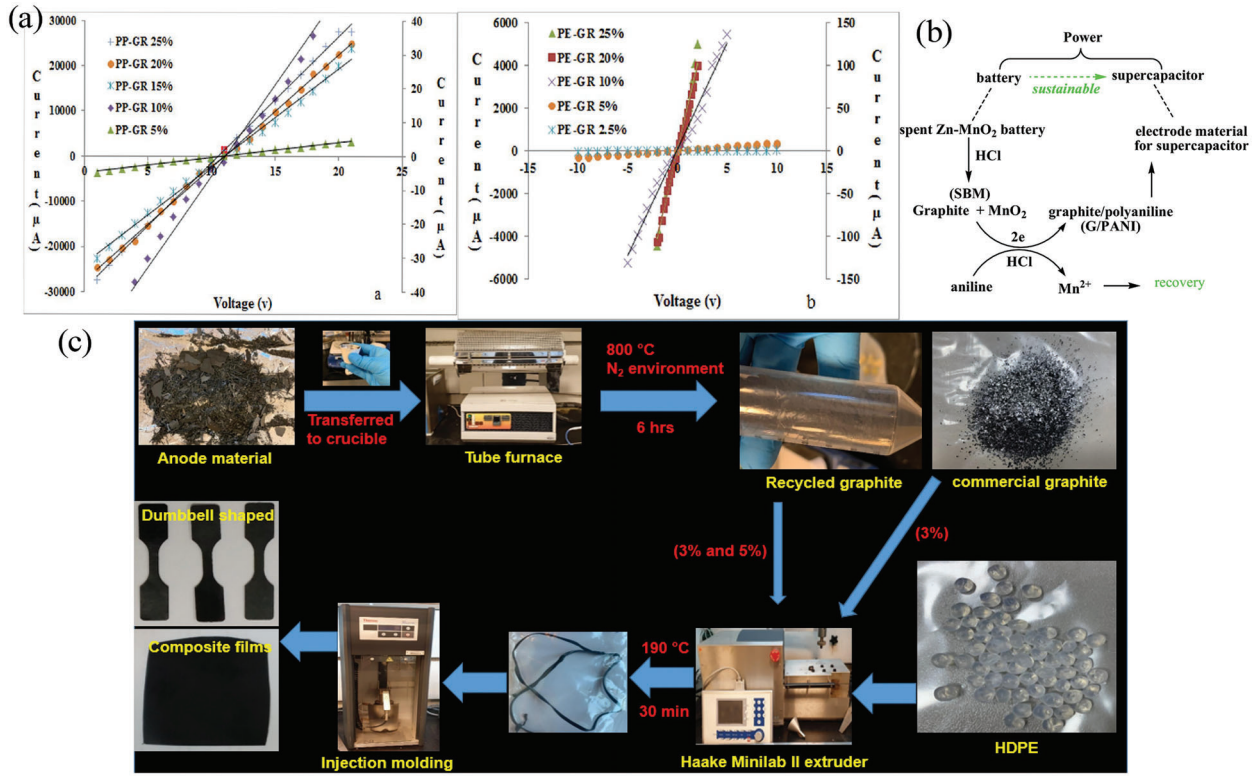

Figure 17. a) I–V plot of waste polypropylene–GRx nanocomposite thin films (left) and waste polyethylene–GRx nanocomposite thin films (right). Reproduced (Adapted) with permission.[126] Copyright@2015, Elsevier. b) Steps involved in the fabrication of HDPE-recycled graphite composite materials. Reproduced (Adapted) with permission.[127] Copyright@2022, Elsevier. c) Proposed principle of "what comes from the power should be used for the power". Reproduced (Adapted) with permission.[128] Copyright@2016, Elsevier.

g^{-1} in SIBs at 0.2 A g^{-1} and 320 mAh g^{-1} in KIBs at 0.05 A g^{-1} (**Figure 18a**).[129] Divya et al. proposed a "solvent-co-insertion" mechanism using ether solvents to achieve a highly reversible Na-intercalation into graphite from spent Li-ion batteries for high-energy Na capacitors. An energy density of 59.93 Wh kg^{-1} with an excellent cycling capability of 5 000 cycles at ambient temperature and a retention rate of ≈98% has been reached with this approach (Figure 18b).[130] Liu et al. utilized a concentrated H_2SO_4 and 750 °C sintering to reconstruct waste graphite for sodium ion batteries with a high reversible capacity of 127 mAh g^{-1} at 50 mA g^{-1} and 90.98% capacity retention after 500 cycles at 2 000 mA g^{-1} (Figure 18c).[131] As emerging state-of-the-art Al-based batteries, the carbon-based cathode material is reversibly intercalated and deintercalated with the chloride aluminate anion ($AlCl_4^-$). The theoretical gravimetric capacity is 2981 mAh g^{-1}. Noteworthy, Pham et al. demonstrated a waste graphite as a good Al^{3+} storage material. The capacity of 124 mAh g^{-1} at 50 mA g^{-1} was recovered, and even after 6 700 cycles at a faster rate of 300 mA g^{-1}, graphite retained 81% of its initial capacity. This excellent aluminum ion storage performance makes recycled graphite a promising cathode material.[132]

4.6. Lithium-Sulfur Batteries

Waste graphite represents also the potential in application as a carrier material for sulfur in lithium-sulfur batteries (LSBs). LSBs with a high energy density have attracted much attention as appealing next-generation ESSs; However, there is a need to overcome the polysulphides shuttle effect and provide the electronic conductivity to insulating sulphur both features leading to a deterioration of battery performance. Thus, the application of carbonaceous materials as sulphur body is gaining attention. Waste graphite can be employed as a carrier for LSBs with suitable modifications, as it can serve as a conductive additive to enhance the performance of LSBs. However, sulfur exhibits limited solubility in graphite, which could potentially restrict its role as a carrier. Yang et al. prepared a spent graphite (SG)/S cathode for lithium-sulfur batteries from SG of end-of-life LIBs. Metal elements such as Ni, Co and Mn were also brought through the dissolution of the active cathode material. These elements increase the conductivity and effectively promote the conversion kinetics of lithium polysulfide (LiPS) in a way that SG effectively adsorbs and immobilizes LiPS, thereby reducing the shuttle effect in lithium-sulfur batteries. In addition, the SG/S cathode with a high sulfur content of 78.4% delivers an initial discharge capacity of 1377 mAh g^{-1} with excellent cyclability stability at a rate of 0.2 C. Even after 500 cycles, the specific capacity is found to be 765 mAh g^{-1} (**Figure 19a**).[136] Xu et al. directly applied the in situ formation of porous structures, defects and polar functional groups of spent graphite as functional intermediate layers to enhance polysulfide capture and catalytic performance of Li-S batteries. High discharge capacity of 68 mAh g^{-1} can be obtained with a low decay rate of 0.08% per cycle out of 500 cycles at 1 C (Figure 19b).[111]

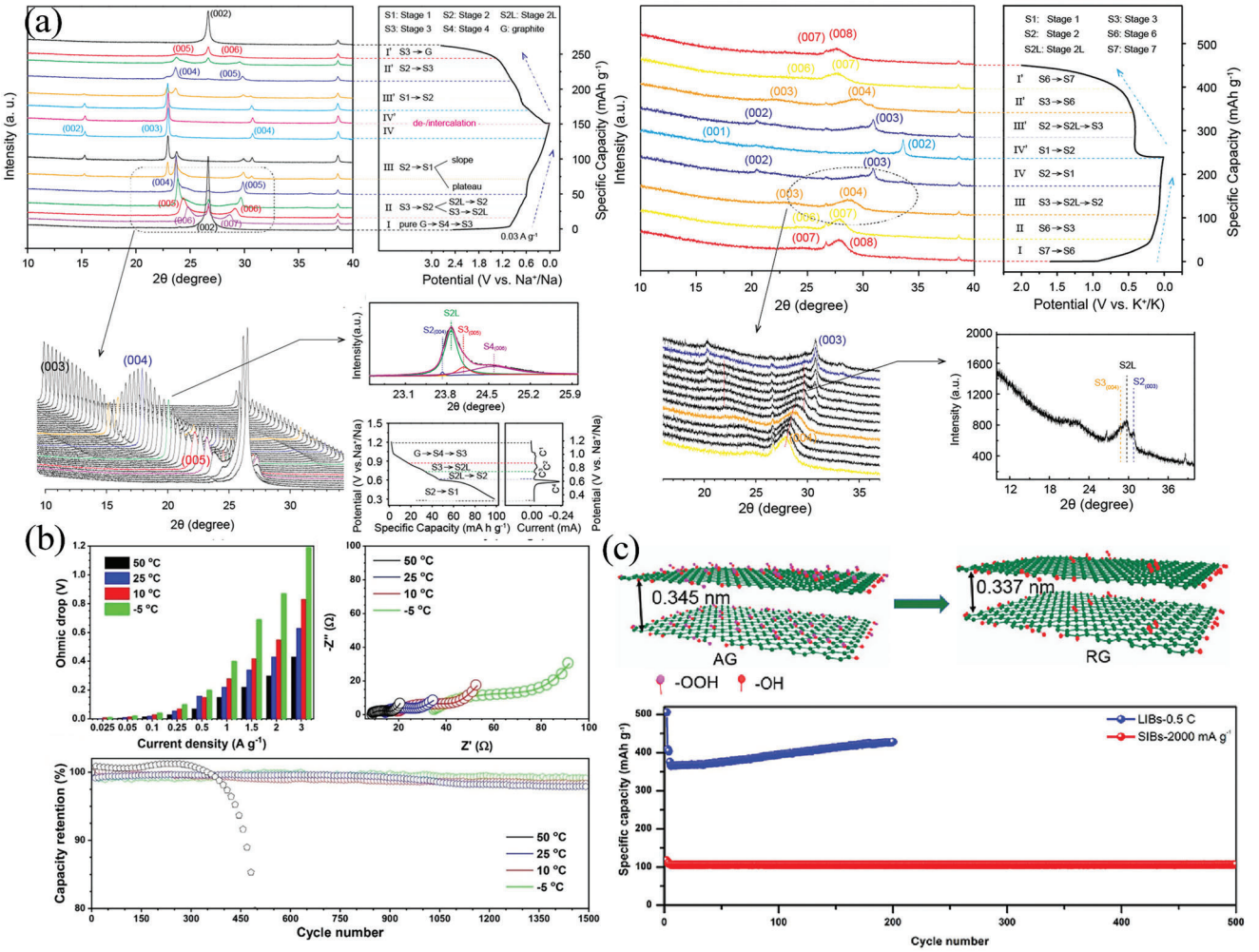

Figure 18. a) In operando XRD patterns and analyses for the structural evolution during the electrochemical de-/intercalation of solvated Na-ions in Na-ion half cells (left), K-ion de-/intercalation in K-ion half cells (right). Reproduced (Adapted) with permission.[129] Copyright@2019, RSC Publishing. b) Effect of temperature on the performance of activated carbon/recovered graphite coin cell assembly with 0.5 M $NaPF_6$ in ether-based electrolyte. Reproduced (Adapted) with permision.[130] Copyright@2020, Wiley-VCH GmbH. c) Long-term cycling performance of sodium ion batteries at 2 000 mA g^{-1} after 500 cycles. Reproduced (Adapted) with permission.[131] Copyright@2020, Elsevier.

Waste graphite is expected to be increasingly involved in lithium-sulfur batteries because of its economic value.

4.7. Adsorbents

Carbon is an important class of absorbents for pollutant removal, and different forms of carbon materials such as graphene,[137,138] activated carbon,[139,140] carbon nanotubes,[141–143] resins[144,145] and expanded graphite[146,147] exhibit different pollution adsorption capacities. Scrap graphite has a strong application prospect feasibility as a key carbon material. Nguyen and Oh et al. prepared ACM from waste graphite which significantly enhanced the oxidation of peroxynitrite with zero-valent iron and the reduction of nitro compounds by DTT and hydrogen sulfide. The results suggest that ACM may be an effective adsorbent and catalyst in the redox process for the remediation of contaminated water and soil.[105] Natarajan et al. recovered mixed metal oxides $LiMn_2O_4$ (MO) and graphite from spent LIBs and re-utilized them as adsorbents for the removal of anionic Congo red (CR) and cationic methylene blue (MB) dyes from aqueous solutions. The results revealed that 1 mg g^{-1} of CR dye, while the adsorption capacity of MO for CR and MB dyes was 7.4 mg g^{-1} and 4.2 mg g^{-1}, respectively. In the case of GO, 100% of MB dyes were adsorbed up to 1 000 mg L^{-1} due to electrostatic interactions of oppositely charged adsorbent-adsorbate species and Π-Π interactions.[148] Zhang et al. synthesized carbon loaded $Mg(OH)_2$ nanoparticles of medium carbon microbeads on the surface of waste graphite, which could be used as an efficient and stable phosphate adsorbent with a sorption capacity of 588.4 mg g^{-1}.[149] Zhang and Yao et al. also prepared MnO_2-modified graphite sorbents from waste graphite for the treatment of Pb, Cd, and Ag contaminated water. Compared with the original artificial graphite, the MnO_2-modified AG decipted significantly higher removal capacity of Pb (II), Cd (II) and Ag (I) with 99.9, 79.7 and 99.8% removal rates, respectively.[150]

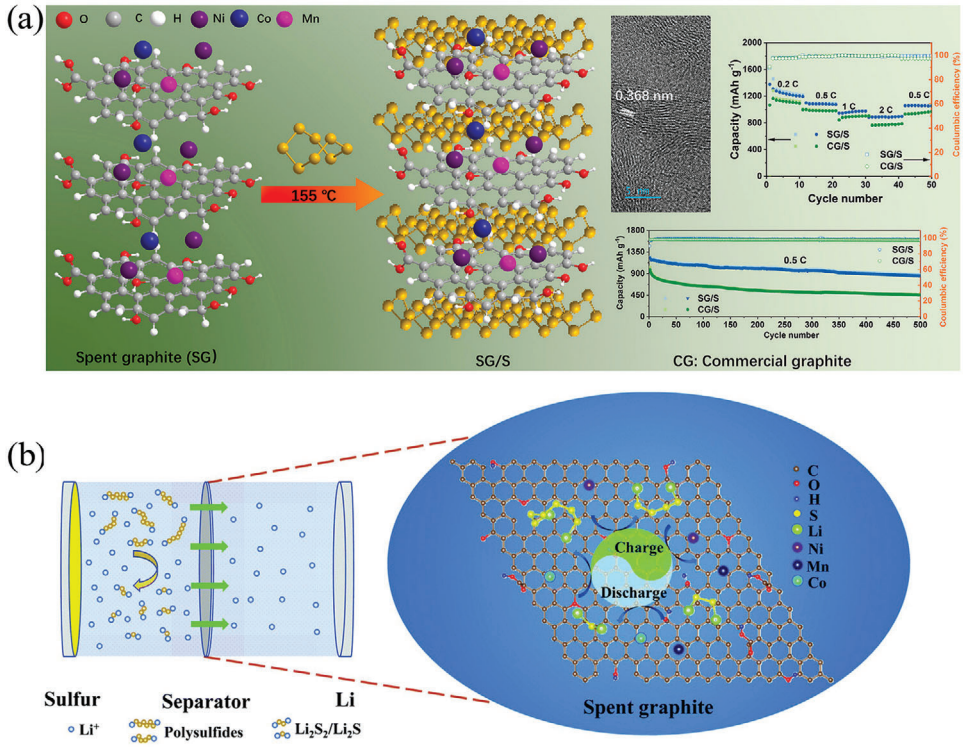

Figure 19. a) Rate capability of SG/S and CG/S electrodes and cycling performances of SG/S and CG/S electrodes at 0.5 C. Reproduced (Adapted) with permission.[136] Copyright@2022, Elsevier. b) A schematic illustration of the adsorption properties and catalytic effects of a SG-modified separator in Li–S batteries. Reproduced (Adapted) with permission.[111] Copyright@2021, Elsevier.

4.8. Silicon/Graphite Composite Anode Material

Lithium-Nickel-Cobalt-Aluminum-Oxide (NCA) and $LiNi_{0.8}Co_{0.1}Mn_{0.1}O_2$ (NCM811) have high-capacity density, but matching with the traditional graphite anode is far from meeting the new generation of high energy density batteries, and only the participation of the most commercially appealing silicon-based anode can match it ($Li_{15}Si_4$ with theoretical capacity of 3 600 mAh g^{-1} and low delithiation voltage 0.4 V vs Li/Li^+). Due to the porous structure and sufficient void space of the treated waste graphite, it can bind well with silicon and effectively mitigate volume expansion. Ruan et al. treated initially spent graphite to prepare low-cost nano silicon-graphite composite involving pitch coating. It exhibited both good cyclability (92.47% capacity retention) and good rate capability (434.1 mAh g^{-1}) over 300 cycles at 500 mA g^{-1} (**Figure 20**a).[151] Xu et al. spontaneously tuned the zeta potential to electrostatically integrate Si nanoparticles into SG matrix so that the defect-enriched SG can effectively improve the conductivity and promote the electrochemical kinetics of the electrode. Moreover, the oxygen-containing functional groups on its surface can modulate the solid electrolyte interfacial components by generating more organic components to enhance its mechanical toughness. It delivered a high initial discharge capacity of 1321.8 mAh g^{-1} at 50 mA g^{-1} and a stable cycle life with a capacity retention of 69% at 1 000 mA g^{-1} after 400 cycles (Figure 20b).[152]

4.9. Reductants for Spent Cathodes

Efficient retrieval of valuable metals nickel, cobalt and manganese from retired LIBs is the core of today's recycling. Clever use of waste graphite as a reducing agent for reductive leaching to extract metals builds a closed-loop pathway to achieve a win-win cooperation. Tang et al. recovered and regenerated $LiCoO_2$ based discarded LIBs by carbon (waste graphite) thermal reduction vacuum pyrolysis, achieving over 93% recovery of Li and over 99% recovery of Co. Finally, the recovered CoO and Li_2CO_3 were used to regenerate $LiCoO_2$, which delivered a specific capacity of 145 mAh/g at 1C and retained 93% of the initial capacity after 100 cycles.[153] Zhang et al. utilized spent graphite roasting combined with H_2SO_4 leaching for the recovery of valuable metals from $LiNi_xCo_yMn_zO_2$. Under optimal conditions, more than 99% of Ni, Co, and Li were extracted and 97% of Mn was leached without the addition of other reducing agents.[154] Pindar et al. investigated the reduction of active cathode materials (pure $LiCoO_2$ and mixed $LiCoO_2$, $LiNi_{0.5}Mn_{1.5}O_4$, $LiMn_2O_4$) at different times, different amounts of waste graphite and activated carbon and microwave power. The final products include Co: 71.6%, Mn: 8.5%, Ni: 6.3%, O: 13.6%, lithium extraction: 82%, and process yield of 32%.[155] Tao et al. used pyrolysis and hydrometallurgical leaching to achieve full-component recovery of spent $LiCoO_2$. During the pyrolysis process, the waste LCO was deconstructed and reduced by the synergistic effect of pyrolysis gas and waste graphite.

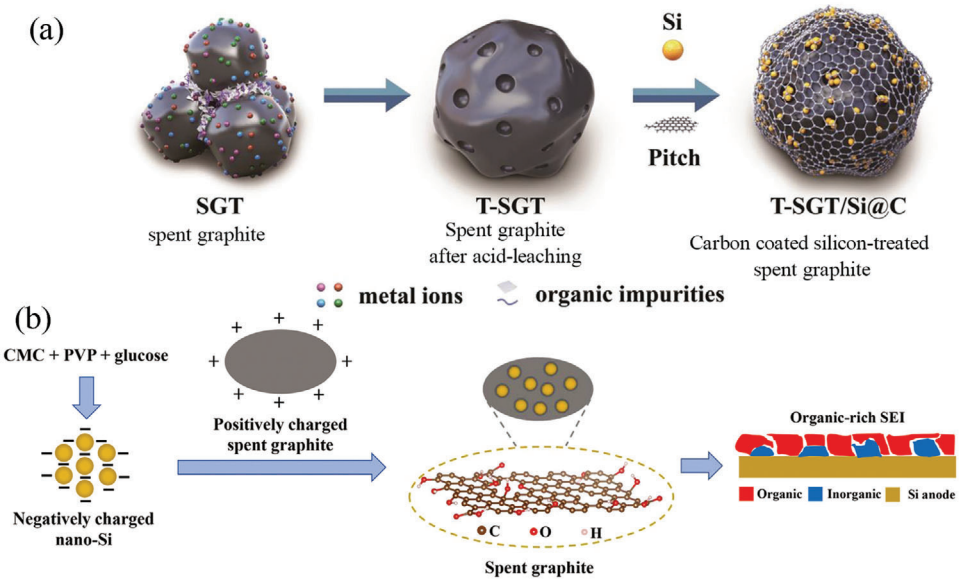

Figure 20. a) Schematic illustration of the preparation process for T-SGT/Si@C anode materials. Reproduced (Adapted) with permission.[151] Copyright@2021, Elsevier. b) Schematic illustration for the preparation and working mechanism of the Si/SG composite. Reproduced (Adapted) with permission.[152] Copyright@2021, Royal Society of Chemistry.

Selective recovery of 87.9% and 99.1% of Li and Co, respectively, was achieved by carbonic acid water leaching and reductant-free acid leaching (**Figure 21**).[156]

4.10. Other Appealing Applications

Beyond the above-mentioned applications, new also developed to repurpose discarded graphite. Surface treatment of battery conductive substrates using functional coatings is a breakthrough technological innovation. A series of carbon materials including nano-graphite flakes and graphene/graphene oxide prepared from waste graphite are uniformly and finely coated on aluminum/copper foil to form the carbon coated aluminum/copper foil. Its numerous merits are as follow: 1) improving the adhesion of active materials and collectors and reducing the cost of electrodes manufacturing; 2) protecting the collector and prolonging the battery life; 3) inhibiting battery polarization, lowering battery

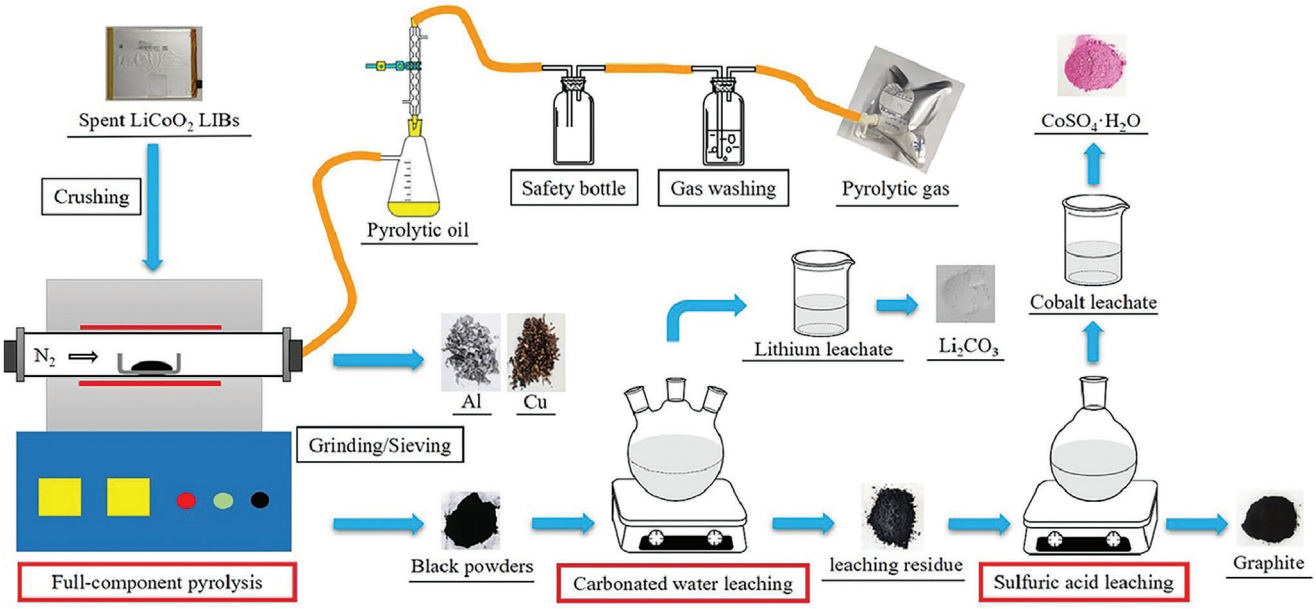

Figure 21. Schematic illustration of recovery of spent LCO via pyrolysis and hydrometallurgical leaching. Reproduced (Adapted) with permission.[156] Copyright@2022, Elsevier.

internal resistance and extending battery cycle life; 4) enhancing the processing performance of battery materials. Apart from Na-ion chemistry, cells based on Mg, Ca are also competitive despite lower specific capacities. Functionalization of the waste graphite surface using heteroatom (N, P, B etc.) doping for catalysis and energy storage. These applications of waste graphite have not been involved yet.

5. Conclusions and Outlook

Considerable value of battery-grade graphite materials is embedded in expired LIBs. Thus, there is an opportunity for graphite recovered from spent batteries to make supply to be balanced with demand, additionally reducing transportation expenses. The graphite content in graphite anodes originating from EVs is above 80%, far higher than the grade of mined graphite. Moreover, in the case of recovered graphite there is no need for the graphitization process over 1 500 °C, what allows saving a significant amount of energy and mitigates expenditure. By introducing the principles of the circular economy, we can significantly reduce costs of a high-quality recycled graphite in comparison to a "new" graphite thereby minimizing secondary environmental impacts. Retrieving and reusing the essential components of anodes and cathodes can potentially lead to lower prices of LIBs and EVs. Furthermore, it is crucial to explore and expand the potential applications of waste graphite anodes in sustainable and valuable ways. Implementing these measures would contribute to a greener future and enhance the feasibility of renewable energy technologies. In the coming years, the growing number of EVs will present a complex challenge for recyclers when it comes to managing e-waste at the end of their lifespan. Several countries in the European Union, North America, and Japan have made significant progress in establishing a global power battery recycling network. Many of these countries have also implemented regulations that oblige battery manufacturers to collect and dispose of expired batteries free of charge for consumers. Currently Umicore, Toxco, Batrec AG, Inmetco, SNAM, Sumitomo-Sony and other companies are implementing tonnage recycling of EoL-LIBs worldwide and unhurriedly improving the complete battery life cycle chain. In general, the recycling of waste lithium-ion batteries (ReLIBs) is a combination of physical and chemical means.[157,158] But still it is mostly dedicated to the extraction of scarce metals from cathodes, and ultimately the real impetus remains the attractively economic value that it embodies. Graphite, on the other hand, has been an important and potentially impoverished resource that has been massively neglected because it does not yield as much profit as cathode material. Recycling of graphite has been considered a relatively new and developing field. The challenge lies in finding economically feasible and innovative methods to restore graphite. It is important to recognize that in the coming decades, there is a risk of shrinking or even depleting graphite reserves, with no suitable alternatives for anode materials. Consequently, recycling of used graphite becomes crucial for the sustainable and green development of batteries.

Based on current global shipments of lithium-ion batteriesand assuming a battery lifetime of eight years, it is estimated that the accumulative amount of waste graphite from these batteries will increase from 95 kt in 2022 to 14 134 kt in 2038. Currently, most recycling efforts focus on recovering valuable metals from the cathodes of LIBs. However, in the future, it is expected that the recycling rate for waste graphite will reach ≈35%. This could lead to a diverse range of applications for recycled graphite, as discussed in this review, with ≈40% being used in secondary manufacturing of LIBs, 30% for making electrode material, 10% for preparing graphene, 9% for sealing material, 9% for refractories, and 2% for catalyst carriers, as shown in **Figure 22**. These projections suggest a potential shift toward more sustainable and varied uses for waste graphite in the LIB recycling industry. We strongly believe that scrap graphite, being the best alternative to pristine graphite, will gain importance with its multiple applications and economic value in the coming years.

The European Union has just implemented new regulations for decommissioned batteries.[160] Concerning recycling and reuse issues, these regulations primarily focus on enhancing the traceability and transparency of retired batteries. Article 71 defines targets for recycling efficiency and recovery of materials from various battery types, for LIBs recycling of 70% by average weight of lithium-based batteries will be compulsory by the end of 2030 (65% by the end of 2027), in line with achieving the targets for recovery of the following elements: 95% of cobalt, 95% of copper, 80% of lithium and 95% of nickel by the end of 2031. Nevertheless, graphite has still not been included in the recovery targets in this regulation.

Tesla is collaborating with various industries to create the Global Battery Alliance (GBA). The goal of GBA is to establish a system called "battery passport" that sets worldwide standards, data, and benchmarks for a sustainable and transparent battery market. This system includes a digital identification for each battery, enabling the tracking of its manufacturing history and facilitating recycling and reuse. Additionally, GBA aims to develop a global management framework that spans across the entire battery value chain.[161]

All in all, the recycling of used batteries and the regeneration of waste graphite represent a series of challenges, but we maintain confidence in their prospects. The primary hurdle involves processing used batteries, with the initial crushing step making it difficult to differentiate the components of the black mass. A promising solution on the horizon is the use of robotic disassembly systems, which have the potential to improve separation efficiency and preserve valuable components. Another challenge relates to the economic and environmental benefits of regenerating waste graphite, especially regarding the efficiency of the hydrometallurgical processes. Although not a new technology, improving its economic viability is a necessary step in recycling waste graphite and could lead to scalability in the future. As we delve deeper into this field, we see positive signs and have high hopes for the future of waste graphite recycling.

Once a recycling technology, that is both standardized and climate-friendly and cost-competitive, is implemented, it will make it possible to embrace the arrival of retired batteries with thoroughly open hands in an era of greatly enlarged demand for secondary rechargeable LIBs. It is important to acknowledge that in any industry, technology alone is not enough; supportive policies play a crucial role. Considering the current state of the industry, we have also provided recommendations from various perspectives.

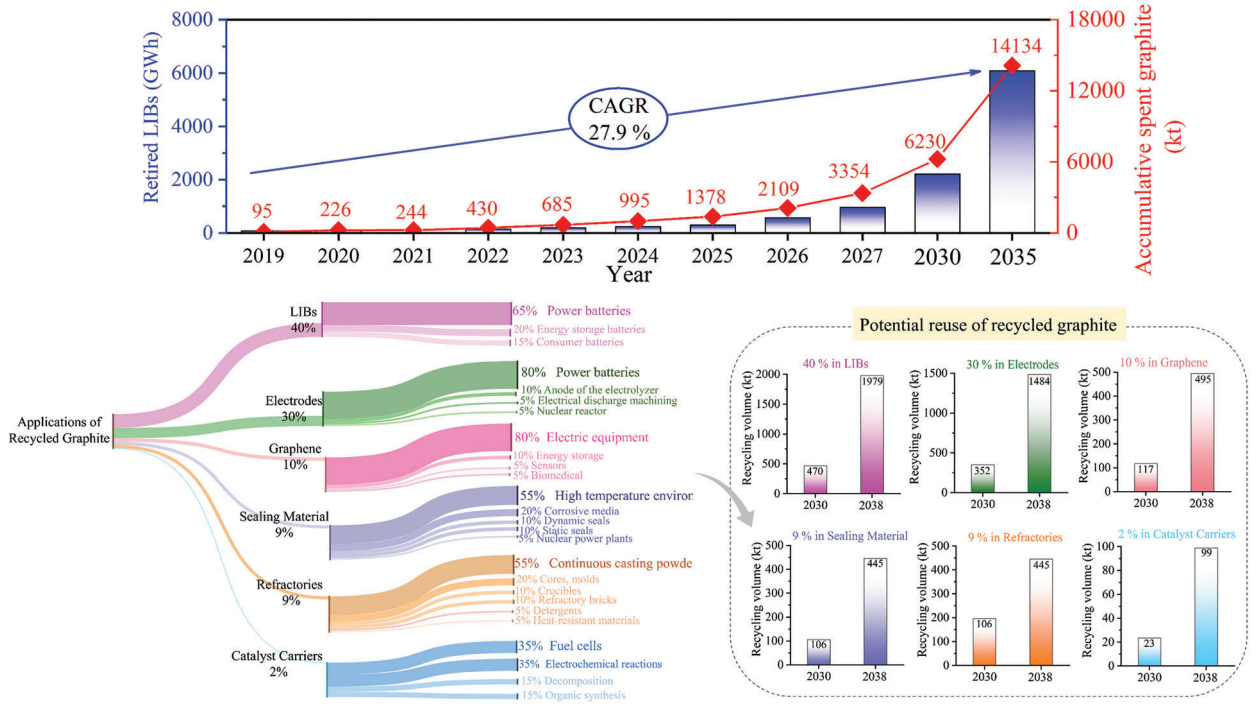

Figure 22. Forecasting of the accumulative waste graphite and the reuse of recovered graphite (CAGR = Compound Annual Growth Rate). The original data represent the worldwide shipments of lithium-ion batteries.[159] Assuming that these batteries have a lifespan of 8 years, the corresponding annual shipments represent the quantity of retired LIBs after 8 years. To illustrate, if the global shipments amounted 957.7 GWh in 2022, then the projected quantity of discarded LIBs will also be 957.7 GWh in 2030. 1 GWh LIBs approximately requires ≈1300 tonnes of anode material. Therefore, the estimated amount of discarded graphite in 2030 is the cumulative sum from 2022 to 2030, resulting in a total discarded quantity of 3 354.39 kilotonnes. We calculated the actual cumulative recovered graphite based on a 35% recycling rate for waste graphite, the actual cumulative amount of recycled graphite is 1174 kt (= 3 354.39 * 35%). We anticipate that 40% of this recycled graphite will be used in the secondary manufacturing of LIBs, resulting in a cumulative recovered quantity of 470 kt (= 1174 * 40%).

In terms of policy, it is essential for the LIBs recycling industry to take advantage of favorable policies and establish management systems and standards for the utilization and recycling of power batteries. This includes implementing regulations and penalties, as well as qualifying and monitoring recycling enterprises to prevent the operation of illicit workshops that falsely claim to support sustainability and decarbonization. These workshops often expose employees to poor working conditions, negatively impacting their health and quality of life. Additionally, regulations should be put in place for the transportation and storage of end-of-life LIBs e-waste to prevent inappropriate disposal through landfilling or incineration.

Regarding technology, efforts should be made by upstream material companies, downstream battery factories, and car companies to establish traceability systems that track the production time and material components of batteries. Utilizing material identification codes on cylindrical cells, such as 18650/21700 cells, can facilitate better sorting techniques for different types of battery materials during recycling, preventing safety issues that arise when lead-acid and LIBs are mixed. Moreover, the piloting of infrastructure such as robot disassembly line can enable the automated separation of cathode and anode materials using adaptable algorithms, ensuring efficient and safe processing without compromising the health of workers. Last, the development of equipment for rapid and accurate diagnosis of the state of healthand state of charge of individual cells will aid in their classification and reorganization, promoting the progressive utilization of LIB e-waste before recycling. Advanced diagnostics embedded in battery management systems can provide valuable data at the end of a battery's useful life.[32]

At the social level, there is a need for a comprehensive e-waste flow management system, particularly as a significant number of used batteries end up in informal small workshops.[162] To address this issue, formal vehicle businesses should establish well-regulated recycling incentive programs to encourage both retailers and individual users to directly hand over their batteries to qualified recycling enterprises instead of disposing of them in household garbage or recycling bins. This integration of the waste recycling industry chain will better contribute to overall development and environmental sustainability. Regarding Europe, these issues are however addressed in Battery Directive[160] and hopefully will be implemented in a near future.

A deeper examination and reflection on the recycling of spent graphite are crucial and are the focus of this review. Addressing these important questions, such as whether large quantities of e-waste are accumulating in abandoned landfills and if there are better alternatives available appear imperative. Additionally, finding sustainable solutions to alleviate the environmental burden caused by land contamination in these abandoned landfills is essential.

Acknowledgements

Honghong Tian kindly acknowledges the financial support by the China Scholarship Council (CSC, No.202009150013). Ralf Riedel and Magdalena Graczyk-Zajac acknowledge the support of HA HessenAgentur GmbH, Innovationsförderung Hessen-Förderung der Elektromobilität, projekt number 849/20-09. Open access funding enabled and organized by Project DEAL.

Open access funding enabled and organized by Projekt DEAL.

Conflict of Interest

The authors declare no conflict of interest.

Author Contributions

Honghong Tian wrote the manuscript. Magdalena Graczyk-Zajac, Alois Kessler, Anke Weidenkaff, and Ralf Riedel revised the manuscript.

Keywords

failure lithium-ion batteries, graphite recycling, recycled graphite applications, retired lithium-ion batteries

Received: August 21, 2023
Revised: October 28, 2023
Published online: December 24, 2023

[1] A. M. P. Sakita, R. Della Noce, P. L. Gastelois, W. A. A. Macedo, R. Lassarote Lavall, *Chem. Eng. J.* **2022**, *427*, 131731.
[2] Y. Machida, N. Matsumoto, T. Isono, K. Behnia, *Science* **2020**, *367*, 309.
[3] S. Wu, T. Li, Z. Tong, J. Chao, T. Zhai, J. Xu, T. Yan, M. Wu, Z. Xu, H. Bao, T. Deng, R. Wang, *Adv. Mater.* **2019**, *31*, 1905099.
[4] C. E. Morstein, A. Klemenz, M. Dienwiebel, M. Moseler, *Nat. Commun.* **2022**, *13*, 1.
[5] P. Restuccia, M. Ferrario, M. C. Righi, *Carbon* **2020**, *156*, 93.
[6] M. Okada, N. Ohta, O. Yoshimoto, M. Tatsumi, M. Inagaki, *Carbon* **2017**, *116*, 737.
[7] H. Jäger, W. Frohs, Online ISBN: 9783527674046, Wiley-VCH, Germany **2021**.
[8] K. S. Novoselov, A. K. Geim, S. V. Morozov, D. Jiang, Y. Zhang, S. V. Dubonos, I. V. Grigorieva, A. A. Firsov, *Science* **2004**, *306*, 666.
[9] H. W. Davidson, H. H. W. Losty, *Nature* **1958**, *181*, 1057.
[10] S. Vinod, C. S. Tiwary, L. D. Machado, S. Ozden, J. Cho, P. Shaw, R. Vajtai, D. S. Galvão, P. M. Ajayan, *Nano Lett.* **2016**, *16*, 1127.
[11] Z. Ma, J. W. Li, T. An, *Conservation and Utilization of Mineral Resources* **2018**, *5*, 1.
[12] Fastmarkets, Prospects for natural graphite flake markets, https://www.tirupatigraphite.co.uk/pdf/Fast-market-Graphite-Market-report.pdf, (accessed: 2018).
[13] a) U.S. Geological Survey, Mineral commodity summaries, https://pubs.usgs.gov/periodicals/mcs2023/mcs2023.pdf, (accessed: 2023). b) U.S. Geological Survey, Mineral Commodity Summaries, https://pubs.usgs.gov/periodicals/mcs2022/mcs2022-graphite.pdf, (accessed: 2022).
[14] a) OEC, Brazil (BRA) exports, imports, and trade partners, https://oec.world/en/profile/country/bra/, (accessed: 2021). b) SYRAH RESOURCES, Balama graphite operation-Syrah, https://www.syrahresources.com.au/our-business/balama-graphite-operation, (accessed: 2022). c) L. Y. Zuo, W. Y. Zhang, Z. Li, *Conservation and Utilization of Mineral Resources* **2019**, *39*, 32; d) BLACK ROCK MINING LIMITED, Black Rock Mining confirms 25% increase in Measured Mineral Resource, now the largest in class globally, https://minedocs.com/23/Mahenge-MRMR-02032022.pdf, (accessed: 2022). e) Mining Technology, Epanko graphite project, https://www.mining-technology.com/projects/epanko-graphite-project/, (accessed: 2015). f). A. M. Arribas R, J. L. Mauk, Metals, minerals, and society (special publication), Society of Economic Geologists (SEG), **2018**, https://doi.org/10.5382/SP.21.15; g) NS ENERGY, Tirupati to acquire Battery Minerals' Mozambique graphite projects, https://www.nsenergybusiness.com/news/tirupati-to-acquire-battery-minerals-mozambique-graphite-projects/, (accessed: 2021).
[15] XURAN, Graphite electrode price-rely on market demand & raw material supply, https://www.graptek.com/technology/quote-information.html, (accessed: 2022).
[16] MMR, Needle coke market-global industry analysis and forecast (2022-2029), https://www.maximizemarketresearch.com/market-report/needle-coke-market/11668/, (accessed: 2022).
[17] S. Alpha, It doesn´t take nerves of steel to buy GrafTech, https://seekingalpha.com/article/4297398-doesnt-take-nerves-of-steel-to-buy-graftech, (accessed: 2019).
[18] Global Electric Vehicle Outlook, https://iea.blob.core.windows.net/assets/e0d2081d-487d-4818-8c59-69b638969f9e/GlobalElectricVehicleOutlook2022.pdf, (accessed: 2022).
[19] M. Drüe, M. Seyring, M. Rettenmayr, *J. Power Sources* **2017**, *353*, 58.
[20] C. Sole, N. E. Drewett, L. J. Hardwick, *Faraday Discuss.* **2014**, *172*, 223.
[21] S. Weng, S. Wu, Z. Liu, G. Yang, X. Liu, X. Zhang, C. Zhang, Q. Liu, Y. Huang, Y. Li, M. N. Ates, D. Su, L. Gu, H. Li, L. Chen, R. Xiao, Z. Wang, X. Wang, *Carbon energy* **2023**, *5*, e224.
[22] a) Seeking Alpha, Graphite miners news, https://seekingalpha.com/article/4549764-graphite-miners-news-month-october-2022, (accessed: 2022); b) RystadEnergy, Synthetic graphite holds the key to meeting battery demand surge, despite ESG concerns, https://www.rystadenergy.com/news/fake-it-till-you-make-it-synthetic-graphite-holds-the-key-to-meeting-battery-dema, (accessed: 2022); c) German Mineral Resources Agency (DERA) Rohstoffinformationen, Supply and demand of natural graphite, (accessed: 2020); d) IPCEI Batteries, Resilient supply chains in the battery industry, https://www.ipcei-batteries.eu/fileadmin/Images/accompanying-research/publications/2023-03-BZF_Studie_Lieferketten-ENG.pdf, (accessed: 2023).
[23] a) MINING.COM, Graphite deficit starting this year, as demand for EV battery anode ingredient exceeds supply, https://www.mining.com/web/graphite-deficit-starting-this-year-as-demand-for-ev-battery-anode-ingredient-exceeds-supply/, (accessed: 2022); b) International Renewable Energy Agency, Geopolitics of the energy transition, https://www.irena.org/Digital-Report/Geopolitics-of-the-Energy-Transition-Critical-Materials (accessed:2022).
[24] N. Niese, C. Pieper, A. Arora, A. Xie, BCG, https://www.bcg.com/en-ca/publications/2020/case-for-circular-economyin-electric-vehicle-batteries, (accessed: 2020).
[25] M. K. Tran, M.-T. F. Rodrigues, K. Kato, G. Babu, P. M. Ajayan, *Nat. Energy* **2019**, *4*, 339.
[26] R. E. Ciez, J. F. Whitacre, *Nat. Sustain.* **2019**, *2*, 148.
[27] C. S. Dos Santos, J. C. Alves, S. P. Da Silva, L. Evangelista Sita, P. R. C. Da Silva, L. C. De Almeida, J. Scarminio, *J. Hazard. Mater* **2019**, *362*, 458.
[28] B. Zhang, H. Xie, B. Lu, X. Chen, P. Xing, J. Qu, Q. Song, H. Yin, *ACS Sustainable Chem. Eng.* **2019**, *7*, 13391.
[29] S. Natarajan, V. Aravindan, *ACS Energy Lett.* **2018**, *3*, 2101.

[30] X.-H. Yue, F.-S Zhang, *Chem. Eng. J.* **2022**, *450*, 138388.
[31] S. Natarajan, V. Aravindan, *Adv. Energy. Mater.* **2020**, *10*, 2002238.
[32] G. Harper, R. Sommerville, E. Kendrick, L. Driscoll, P. Slater, R. Stolkin, A. Walton, P. Christensen, O. Heidrich, S. Lambert, A. Abbott, K. Ryder, L. Gaines, P. Anderson, *Nature* **2019**, *575*, 75.
[33] Forbes, Batteries are the next environmental challenge, https://www.forbes.com/sites/miltonezrati/2021/07/25/batteries-are-the-next-environmental-challenge/?sh=1cee8a583caa, (accessed: 2021).
[34] R. international, At least one scrap fire every week in Germany, https://recyclinginternational.com/business/at-least-one-scrap-fire-every-week-in-germany/28831/, (accessed: 2019).
[35] W. Mrozik, M. A. Rajaeifar, O. Heidrich, P. Christensen, *Energy Environ. Sci.* **2021**, *14*, 6099.
[36] E. Peled, *J. Electrochem. Soc.* **1979**, *126*, 2047.
[37] J. Chen, X. Fan, Q. Li, H. Yang, M. R Khoshi, Y. Xu, S. Hwang, L. Chen, X. Ji, C. Yang, H. He, C. Wang, E. Garfunkel, D. Su, O. Borodin, C. Wang, *Nat. Energy* **2020**, *5*, 386.
[38] B. Han, Z. Zhang, Y. Zou, K. Xu, G. Xu, H. Wang, H. Meng, Y. Deng, J. Li, M. Gu, *Adv. Mater.* **2021**, *33*, 2100404.
[39] P. Zhang, T. Yuan, Y. Pang, C. Peng, J. Yang, Z.-F Ma, S. Zheng, *J. Electrochem. Soc.* **2019**, *166*, A5489.
[40] A. Sarkar, I. C. Nlebedim, P. Shrotriya, *J. Power Sources* **2021**, *502*, 229145.
[41] R. Deshpande, M. Verbrugge, Y.-T. Cheng, J. Wang, P. Liu, *J. Electrochem. Soc.* **2012**, *159*, A1730.
[42] K. Takahashi, V. Srinivasan, *J. Electrochem. Soc.* **2015**, *162*, A635.
[43] W. Xu, C. Welty, M. R. Peterson, J. A. Read, N. P. Stadie, *J. Electrochem. Soc.* **2022**, *169*, 010531.
[44] G. Kwak, J. Park, J. Lee, S. Kim, I. Jung, *J. Power Sources* **2007**, *174*, 484.
[45] G. Rong, X. Zhang, W. Zhao, Y. Qiu, M. Liu, F. Ye, Y. Xu, J. Chen, Y. Hou, W. Li, W. Duan, Y. Zhang, *Adv. Mater.* **2017**, *29*, 1606187.
[46] M. Zier, F. Scheiba, S. Oswald, J. Thomas, D. Goers, T. Scherer, M. Klose, H. Ehrenberg, J. Eckert, *J. Power Sources* **2014**, *266*, 198.
[47] H. G. Lee, S. Y. Kim, J. S. Lee, *npj Comput. Mater.* **2022**, *8*, 103.
[48] B. Song, I. Dhiman, J. C. Carothers, G. M. Veith, J. Liu, H. Z. Bilheux, A. Huq, *ACS Energy Lett.* **2019**, *4*, 2402.
[49] P. Bai, J. Li, F. R. Brushett, M. Z. Bazant, *Energy Environ. Sci.* **2016**, *9*, 3221.
[50] P. Bai, J. Guo, M. Wang, A. Kushima, L. Su, J. Li, F. R. Brushett, M. Z. Bazant, *Joule* **2018**, *2*, 2434.
[51] C. Shen, G. Hu, L.-Z. Cheong, S. Huang, J.-G Zhang, D. Wang, *Small Methods* **2017**, *2*, 1700298.
[52] J. Luo, C.-E. Wu, L.-Y. Su, S.-S. Huang, C.-C. Fang, Y.-S. Wu, J. Chou, N.-L. Wu, *J. Power Sources* **2018**, *406*, 63.
[53] S. Wang, K. Rafiz, J. Liu, Y. Jin, J. Y. S. Lin, *Sustainable Energy Fuels* **2020**, *4*, 2342.
[54] J.-L. Pan, Z. Zhang, M.-L. Zhou, J.-C. Wei, W.-D. He, Z-Y. Yang, *Cellulose* **2021**, *28*, 10579.
[55] X.-B. Cheng, M.-Q. Zhao, C. Chen, A. Pentecost, K. Maleski, T. Mathis, X.-Q. Zhang, Q. Zhang, J. Jiang, Y. Gogotsi, *Nat. Commun.* **2017**, *8*, 1.
[56] S. Bhattacharya, A. R Riahi, A. T. Alpas, *J. Power Sources* **2011**, *196*, 8719.
[57] D. Liu, Y. Wang, Y. Xie, L. He, J. Chen, K. Wu, R. Xu, Y. Gao, *J. Power Sources* **2013**, *232*, 29.
[58] N. Lin, Z. Jia, Z. Wang, H. Zhao, G. Ai, X. Song, Y. Bai, V. Battaglia, C. Sun, J. Qiao, K. Wu, G. Liu, *J. Power Sources* **2017**, *365*, 235.
[59] Y. Wang, H. Li, Z. Wang, C. Lian, Z. Xie, *J. Energy Storage* **2021**, *43*, 103214.
[60] J. Marin-Montin, M. Zurita-Gotor, F. Montero-Chacón, *Materials* **2022**, *15*, 3979.
[61] J. Vetter, P. Novák, M. R. Wagner, C. Veit, K.-C. Möller, J. O. Besenhard, M. Winter, M. Wohlfahrt-Mehrens, C. Vogler, A. Hammouche, *J. Power Sources* **2005**, *147*, 269.
[62] J. Chen, X. Wang, H. Gao, S. Yan, S. Chen, X. Liu, X. Hu, *Surf. Coat. Technol.* **2021**, *410*, 126881.
[63] J. Huesker, L. Froböse, A. Kwade, M. Winter, T. Placke, *Electrochim. Acta.* **2017**, *257*, 423.
[64] J. Landesfeind, A. Eldiven, H. A. Gasteiger, *J. Electrochem. Soc.* **2018**, *165*, A1122.
[65] F. Jeschull, J. Maibach, *Electrochem. Commun.* **2020**, *121*, 106874.
[66] C. Kupper, B. Weißhar, S. Rißmann, W. G. Bessler, *J. Electrochem. Soc.* **2018**, *165*, A3468.
[67] D. H. Jeon, *Energy Storage Mater.* **2019**, *18*, 139.
[68] A. Davoodabadi, J. Li, Y. Liang, D. L. Wood, T. J. Singler, C. Jin, *J. Power Sources* **2019**, *424*, 193.
[69] P. Ma, P. Mirmira, P. J. Eng, S.-B. Son, I. D. Bloom, A. S. Filatov, C. V. Amanchukwu, *Energy Environ. Sci.* **2022**, *15*, 4823.
[70] I. Rey, C. Vallejo, G. Santiago, M. Iturrondobeitia, E. Lizundia, *ACS Sustainable Chem. Eng.* **2021**, *9*, 14488.
[71] a) M. C. C. Lima, L. P. Pontes, A. S. M. Vasconcelos, W. De Araujo Silva Junior, K. Wu, *Energies* **2022**, *15*, 2203; b) Q. Dai, J. Spangenberger, S. Ahmed, L. Gaines, J. C. Kelly, M. Wang, *EverBatt: A Closed-loop Battery Recycling Cost and Environmental Impacts Model*, Argonne National Laboratory, USA, **2019**, https://publications.anl.gov/anlpubs/2019/07/153050.pdf, (accessed: 2019).
[72] a) R. Sojka, Q. Y. Pan, L. Billmann, Comparative study of Li-ion battery recycling processes. ACCUREC Recycling GmbH, Krefeld, Germany, https://pdf4pro.com/view/comparative-study-of-li-ion-battery-recycling-processes-63504c.html, (accessed: 2020). b) L. L. Gaines, Argonne National Laboratory, How Analysis Helps Guide Battery Recycling R&D at the ReCell Center, UL Battery Safety Science Webinar Series, https://ul.org/sites/default/files/2021-07/Gaines%20ReCell%20Center%20UL.pdf, (accessed: 2021).
[73] GRAPHMATECH, A breakthrough in battery recycling helps enable the green transition, https://graphmatech.com/a-breakthrough-in-battery-recycling-helps-enable-the-green-transition/, (accessed: 2022).
[74] Eqs news, EcoGraf Limited, Agreement with leading lithium-ion battery recycler located in South Korea, https://www.eqs-news.com/de/news/corporate/ecograf-limited-agreement-with-leading-lithium-ion-battery-recycler-located-in-south-korea/1403111, (accessed: 2020).
[75] Electrive.com, Panasonic plans Tesla round cells with more recycled content, https://www.electrive.com/2022/01/05/panasonic-plans-tesla-round-cells-with-more-recycled-content/, (accessed: 2022).
[76] J. Xiao, J. Guo, L. Zhan, Z. Xu, *J. Clean. Prod.* **2020**, *255*, 120064.
[77] Y. He, T. Zhang, F. Wang, G. Zhang, W. Zhang, J. Wang, *J. Clean. Prod.* **2017**, *143*, 319.
[78] G. Zhang, Y. He, H. Wang, Y. Feng, W. Xie, X. Zhu, *J. Clean. Prod.* **2019**, *231*, 1418.
[79] N. Cao, Y. Zhang, L. Chen, W. Chu, Y. Huang, Y. Jia, M. Wang, *J. Power Sources* **2021**, *483*, 229163.
[80] Y. Gao, J. Zhang, H. Jin, G. Liang, L. Ma, Y. Chen, C. Wang, *Carbon.* **2022**, *189*, 493.
[81] Z. Zhang, X. Zhu, H. Hou, L. Tang, J. Xiao, Q. Zhong, *Waste Manag.* **2022**, *150*, 30.
[82] H. Tian, M. Graczyk-Zajac, D. M. De Carolis, C. Tian, E. I. Ricohermoso, Z. Yang, W. Li, M. Wilamowska-Zawlocka, J. P. Hofmann, A. Weidenkaff, R. Riedel, *J. Hazard. Mater.* **2023**, *445*, 130607.
[83] X. Ma, M. Chen, B. Chen, Z. Meng, Y. Wang, *ACS Sustainable Chem. Eng.* **2019**, *7*, 19732.

[84] J. Zhang, X. Li, D. Song, Y. Miao, J. Song, L. Zhang, *J. Power Sources* **2018**, *390*, 38.
[85] W. Zhang, Z. Liu, J. Xia, F. Li, W. He, G. Li, J. Huang, *Front. Environ. Sci. Eng.* **2017**, *11*, 1.
[86] A. Goodisman, Y. Jain, D. B. Kwon, *Senior Design Reports (CEB)* **2020**, *128*, https://repository.upenn.edu/cbe_sdr/128.
[87] B. Markey, M. Zhang, I. Robb, P. Xu, H. Gao, D. Zhang, J. Holoubek, D. Xia, Y. Zhao, J. Guo, M. Cai, Y. S. Meng, Z. Chen, *J. Electrochem. Soc.* **2020**, *167*, 160511.
[88] Z. Ma, Y. Zhuang, Y. Deng, X. Song, X. Zuo, X. Xiao, J. Nan, *J. Power Sources* **2018**, *376*, 91.
[89] H. Wang, Y. Huang, C. Huang, X. Wang, K. Wang, H. Chen, S. Liu, Y. Wu, K. Xu, W. Li, *Electrochim. Acta* **2019**, *313*, 423.
[90] Y. Guo, F. Li, H. Zhu, G. Li, J. Huang, W. He, *Waste Manag.* **2016**, *51*, 227.
[91] Y. Yang, S. Song, S. Lei, W. Sun, H. Hou, F. Jiang, X. Ji, W. Zhao, Y. Hu, *Waste Manag.* **2019**, *85*, 529.
[92] Z. Cao, X. Zheng, H. Cao, H. Zhao, Z. Sun, Z. Guo, K. Wang, B. Zhou, *J. Chem. Eng.* **2018**, *337*, 256.
[93] J. Yang, E. Fan, J. Lin, F. Arshad, X. Zhang, H. Wang, F. Wu, R. Chen, L. Li, *ACS Appl. Energy Mater.* **2021**, *4*, 6261.
[94] B. Moradi, G. G. Botte, *J. Appl. Electrochem.* **2016**, *46*, 123.
[95] C. Yi, Y. Yang, T. Zhang, X. Wu, W. Sun, L. Yi, *J. Clean. Prod.* **2020**, *277*, 123585.
[96] H. Yu, H. Dai, Y. Zhu, H. Hu, R. Zhao, B. Wu, D. Chen, *J. Power Sources* **2021**, *481*, 229159.
[97] F. A. Kayakool, B. Gangaja, S. Nair, D. Santhanagopalan, *Sustainable Mater. Technol.* **2021**, *28*, e00262.
[98] Y. Xiao, J. Li, W. Huang, L. Wang, J. Luo, *J. Mater. Sci.: Mater. Electron.* **2022**, *33*, 16740.
[99] Y. Gao, J. Zhang, Y. Chen, C. Wang, *Surf. Interfaces* **2021**, *24*, 101089.
[100] C. Yi, P. Ge, X. Wu, W. Sun, Y. Yang, *J. Energy Chem.* **2022**, *72*, 97
[101] S. Rothermel, M. Evertz, J. Kasnatscheew, X. Qi, M. Grützke, M. Winter, S. Nowak, *ChemSusChem* **2016**, *9*, 3473.
[102] C. Yuwen, B. Liu, H. Zhang, S. Tian, L. Zhang, S. Guo, B. Zhou, *J. Clean. Prod.* **2022**, *333*, 130197.
[103] Y. Zhao, H. Wang, X. Li, X. Yuan, L. Jiang, X. Chen, *J. Hazard. Mater.* **2021**, *420*, 126552.
[104] K. Liivand, M. Kazemi, P. Walke, V. Mikli, M. Uibu, D. D. Macdonald, I. Kruusenberg, *ChemSusChem* **2020**, *14*, 1103.
[105] T.-H. Anh Nguyen, S.-Y. Oh, *Waste Manag.* **2021**, *120*, 755.
[106] Y. Wang, H. Cao, L. Chen, C. Chen, X. Duan, Y. Xie, W. Song, H. Sun, S. Wang, *Appl. Catal., B* **2018**, *229*, 71.
[107] D. Ruan, K. Zou, K. Du, F. Wang, L. Wu, Z. Zhang, X. Wu, G. Hu, *ChemCatChem* **2021**, *13*, 2025.
[108] S. Chen, F. Long, G. Gao, C. Belver, Z. Li, Z. Li, J. Guan, Y. Guo, J. Bedia, *Sep. Purif. Technol.* **2022**, *286*, 120466.
[109] Z. Cao, X. Zheng, H. Cao, H. Zhao, Z. Sun, Z. Guo, K. Wang, B. Zhou, *Chem. Eng. J.* **2018**, *337*, 256.
[110] W. Zhang, Z. Liu, C. Xu, W. He, G. Li, J. Huang, H. Zhu, *Res. Chem. Intermed.* **2018**, *44*, 5075.
[111] Q. Xu, Y. Wang, X. Shi, Y. Zhong, Z. Wu, Y. Song, G. Wang, Y. Liu, B. Zhong, X. Guo, *Green Chem.* **2021**, *23*, 942.
[112] S. Natarajan, H. C. Bajaj, V. Aravindan, *J. Mater. Chem. A* **2019**, *7*, 3244.
[113] K. He, Z.-Y. Zhang, F.-S Zhang, *Waste Manag.* **2021**, *124*, 283.
[114] M. F. El-Kady, M. Ihns, M. Li, J. Y. Hwang, M. F. Mousavi, L. Chaney, A. T. Lech, R. B. Kaner, *Proc. Natl. Acad. Sci. U. S. A.* **2015**, *112*, 4233.
[115] Y. Xu, Z. Lin, X. Zhong, X. Huang, N. O. Weiss, Y. Huang, X. Duan, *Nat. Commun.* **2014**, *5*, 1.
[116] M. F. El-Kady, Y. Shao, R. B. Kaner, *Nat. Rev. Mater.* **2016**, *1*, 1.
[117] Y. Shao, M. F. El-Kady, L. J. Wang, Q. Zhang, Y. Li, H. Wang, M. F. Mousavi, R. B. Kaner, *Chem. Soc. Rev.* **2015**, *44*, 3639.
[118] E. G. Da Silveira Firmiano, A. C. Rabelo, C. J. Dalmaschio, A. N. Pinheiro, E. C. Pereira, W. H. Schreiner, E. R. Leite, *Adv. Energy Mater.* **2013**, *4*, 1301380.
[119] S. Natarajan, S. Rao Ede, H. C. Bajaj, S. Kundu, *Colloids Surf. A: Physicochem. Eng. Asp.* **2018**, *543*, 98.
[120] S. Natarajan, K. Krishnamoorthy, S.-J. Kim, *J. Hazard. Mater.* **2022**, *430*, 128496.
[121] K. K. Jena, A. T. Mayyas, B. Mohanty, B. K. Jena, J. R. Jos, A. Alfantazi, B. Chakraborty, A. A. Almarzooqi, *Energy Fuels* **2022**, *36*, 2159.
[122] C. Iffelsberger, C. W. Jellett, M. Pumera, *Small* **2021**, *17*, 2101233.
[123] B. Wei, L. Zhang, S. Yang, *Chem. Eng. J.* **2021**, *404*, 126437.
[124] S. Ng, K. Ghosh, J. Vyskocil, M. Pumera, *Chem. Eng. J.* **2022**, *435*, 135131.
[125] P. Wang, J. Zhang, L. Dong, C. Sun, X. Zhao, Y. Ruan, H. Lu, *Chem. Mater.* **2017**, *29*, 3412.
[126] S. Natarajan, D. Shanthana Lakshmi, H. C. Bajaj, D. N. Srivastava, *J. Environ. Chem. Eng.* **2015**, *3*, 2538.
[127] K. K. Jena, A. Alfantazi, A. T. Mayyas, *Chem. Eng. J.* **2022**, *430*, 132667.
[128] X. Duan, J. Deng, X. Wang, J. Guo, P. Liu, *J. Hazard. Mater.* **2016**, *312*, 319.
[129] H.-J. Liang, B.-H. Hou, W.-H. Li, Q.-L. Ning, X. Yang, Z.-Y. Gu, X.-J. Nie, G. Wang, X.-L. Wu, *Energy Environ. Sci.* **2019**, *12*, 3575.
[130] M. L. Divya, S. Natarajan, Y.-S. Lee, V. Aravindan, *ChemSusChem* **2020**, *13*, 5654.
[131] K. Liu, S. Yang, L. Luo, Q. Pan, P. Zhang, Y. Huang, F. Zheng, H. Wang, Q. Li, *Electrochim. Acta.* **2020**, *356*, 136856.
[132] H. D. Pham, M. Horn, J. F. S. Fernando, R. Patil, M. Phadatare, D. Golberg, H. Olin, D. P. Dubal, *Sustainable. Mater. Technol.* **2020**, *26*, e00230.
[133] Y. Gao, C. Wang, J. Zhang, Q. Jing, B. Ma, Y. Chen, W. Zhang, *ACS Sustainable Chem. Eng.* **2020**, *8*, 9447.
[134] D. Ruan, F. Wang, L. Wu, K. Du, Z. Zhang, K. Zou, X. Wu, G. Hu, *New J. Chem.* **2021**, *45*, 1535.
[135] Y. Gao, C. Wang, J. Zhang, Q. Jing, B. Ma, Y. Chen, W. Zhang, *ACS Sustainable Chem. Eng.* **2020**, *8*, 9447.
[136] X. Yang, R. Li, J. Yang, H. Liu, T. Luo, X. Wang, L. Yang, *Carbon* **2022**, *199*, 215.
[137] R. Gusain, N. Kumar, S. S. Ray, *Coord. Chem. Rev.* **2020**, *405*, 213111.
[138] Y. Sun, F. Yu, C. Li, X. Dai, J. Ma, *Nano-Micro Lett.* **2020**, *12*, 1.
[139] G. De Falco, M. Barczak, F. Montagnaro, T. J. Bandosz, *ACS Appl. Mater. Interfaces* **2018**, *10*, 8066.
[140] M. Rozwadowski, R. Wojsz, J. Siedlewski, K. E. Wis'Niewski, *Carbon* **1983**, *21*, 209.
[141] Y. Ma, L. Yang, L. Wu, P. Li, X. Qi, L. He, S. Cui, Y. Ding, Z. Zhang, *Sci. Total Environ.* **2020**, *718*, 137299.
[142] A. Kayvani Fard, T. Rhadfi, G. Mckay, M. Al-Marri, A. Abdala, N. Hilal, M. A. Hussien, *Chem. Eng. J.* **2016**, *293*, 90.
[143] M. Barrejón, Z. Syrgiannis, M. Burian, S. Bosi, T. Montini, P. Fornasiero, H. Amenitsch, M. Prato, *ACS Appl. Mater. Interfaces* **2019**, *11*, 12920.
[144] K. Nakakubo, H. Hasegawa, M. Ito, K. Yamazaki, M. Miyaguchi, F. B. Biswas, T. Ikai, K. Maeda, *J. Hazard. Mater.* **2019**, *380*, 120816.
[145] C. Pevida, T. C. Drage, C. E. Snape, *Carbon* **2008**, *46*, 1464.
[146] S. Li, S. Tian, C. Du, C. He, C. Cen, Y. Xiong, *Chem. Eng. J.* **2010**, *162*, 546.

[147] M. Zheng, J. Wang, D. Fu, B. Ren, X. Song, K. Kan, X. Zhang, *J. Hazard. Mater.* **2023**, *442*, 130068.
[148] S. Natarajan, H. C. Bajaj, *J. Environ. Chem. Eng.* **2016**, *4*, 4631.
[149] Y. Zhang, X. Guo, F. Wu, Y. Yao, Y. Yuan, X. Bi, X. Luo, R. Shahbazian-Yassar, C. Zhang, K. Amine, *ACS Appl. Mater. Interfaces* **2016**, *8*, 21315.
[150] T. Zhao, Y. Yao, M. Wang, R. Chen, Y. Yu, F. Wu, C. Zhang, *ACS Appl. Mater. Interfaces* **2017**, *9*, 25369.
[151] D. Ruan, L. Wu, F. Wang, K. Du, Z. Zhang, K. Zou, X. Wu, G. Hu, *J. Electroanal. Chem* **2021**, *884*, 115073.
[152] Q. Xu, Q. Wang, D. Chen, Y. Zhong, Z. Wu, Y. Song, G. Wang, Y. Liu, B. Zhong, X. Guo, *Green Chem.* **2021**, *23*, 4531.
[153] Y. Tang, H. Xie, B. Zhang, X. Chen, Z. Zhao, J. Qu, P. Xing, H. Yin, *Waste Manag.* **2019**, *97*, 140.
[154] Y. Zhang, W. Wang, Q. Fang, S. Xu, *Waste Manag.* **2020**, *102*, 847.
[155] S. Pindar, N. Dhawan, *Sustainable Mater. Technol.* **2020**, *25*, e00157.
[156] R. Tao, P. Xing, H. Li, Z. Sun, Y. Wu, *Resour., Conserv. Recycl.* **2022**, *176*, 105921.
[157] M. Abdollahifar, S. Doose, H. Cavers, A. Kwade, *Adv. Mater. Technol.* **2023**, *8*, 2200368.
[158] L. Gaines, J. Zhang, X. He, J. Bouchard, H. E. Melin, *Batteries* **2023**, *9*, 360.
[159] EVTank, Global Lithium Battery Shipments 957.7GWh in 2022, Energy Storage Battery Growth Outpaces Power Battery, https://www.itdcw.com/news/hangyebaogao/011G332922023.html, (accessed: 2023).
[160] The European Parliament, Regulation of the European Parliament and of the Council Concerning Batteries and Waste Batteries, Amending Directive 2008/98/EC and Regulation (EU) 2019/1020 and Repealing Directive 2006/66/EC, https://data.consilium.europa.eu/doc/document/PE-2-2023-INIT/en/pdf, (accessed: 2023).
[161] Tesla, Tesla Impact report, https://www.tesla.com/ns_videos/2021-tesla-impact-report.pdf, (accessed: 2021).
[162] E.-W. Monitor, V. Forti, C. P. Baldé, R. Kuehr, G. Bel, The global e-waste monitor, https://ewastemonitor.info/wp-content/uploads/2020/11/GEM_2020_def_july1_low.pdf, (accessed: 2020).

Honghong Tian holds a master degree in Inorganic Chemistry from Northwest University in Xi´an, China in 2018 and is currently a Ph.D. student in the Disperse Solids department, Institute of Materials Science, Technical University of Darmstadt. She works under the supervision of Prof. Ralf Riedel and Dr. Magdalena Graczyk-Zajac. Her current research interests include the recycling and regeneration of spent lithium-ion battery materials and their application in energy storage devices.

Magdalena Graczyk-Zajac is an R&D Project Leader in EnBW Energie Baden-Württemberg AG in Karlsruhe, Germany. She works on optimization and efficient operation of stationary storage installations including testing and evaluation of innovative storage solutions. She is also involved in the activities of EnBW related to the extraction of lithium from geothermal sources. She is a deputy coordinator of the Horizon 2020 EU granted project SIMBA (Sodium Ion and Sodium Metal Batteries, Grant Agreement no. 963 542). From September 2023 she holds a Guest Professorship in Materials and Resources Division, Material Science Department of TU Darmstadt. Her research interests include innovative processing routes to obtain well-performing materials for lithium and beyond lithium technologies as well as advanced recycling routes of Li-ion batteries. Magda studied Chemistry at Technical University of Gdansk in Poland and received her Ph.D. in Physical Chemistry on electroactivity of organometallics-modified conducting polymers at Burgundy University, Dijon, France in 2007. Then she moved to CEA Liten Grenoble, France to work as a research engineer on novel electrode and electrolytes for Li-ion batteries. Later, she moved back to academia and continued her research on polymer-derived ceramics for energy-related applications as a postdoc and later Junior Group Leader in Material Science Department of TU Darmstadt, Germany. In May 2020 she joined the R&D division of EnBW.

Alois Kessler born 1965, academic studies of mechanical engineering and graduation in material mechanics at the University of Stuttgart. From 1992 to 2000 plant engineer in the nuclear field at EVS and EnBW. Avocational studies of business administration at IBW Würzburg from 1999 to 2001. Since 2000 Senior Manager and since 2015 Team Manager with focus on decentralized energy systems, renewable energy, energy storage and energy efficiency in the Research and Development Department of EnBW AG in Karlsruhe. From 2012 to 2021, visiting lecturer of industrial energy efficiency at the University of Stuttgart.

Anke Weidenkaff has been head of Fraunhofer IWKS in Hanau and Alzenau Since October 1, 2018. In addition, Anke Weidenkaff is professor at the Technical University of Darmstadt. Her principal areas of research and expertise are materials science and resource strategies, including the development, synthesis and characterization of sustainable materials for energy conversion and storage. Her current work focuses on regenerative, self-healing materials and the development of next-generation process technologies for fast and efficiently closed material cycles. Prof. Dr. Anke Weidenkaff completed her Ph.D. degree in Chemistry at ETH Zürich in 2000, received the Venia Legendi for Solid State Chemistry and Materials Science from the University of Augsburg in 2006 and became section head at Empa as well as associated professor at the University of Bern, Switzerland. She was chair holder for Materials Chemistry and director of the Institute for Materials Science at the University of Stuttgart from 2013–2018, was president of the European Thermoelectric Society (ETS), elected member of the E-MRS Executive Committee and chair of the E-MRS spring meeting 2019. In 2011, she was awarded the Kavli Foundation Lectureship prize. Since 2020, Prof. Dr. Anke Weidenkaff has been a member of the German Advisory Council on Global Environmental Change (WBGU) and since January 2023 a member of the Leopoldina, the German Academy of Natural Scientists.

Ralf Riedel got a Ph.D. degree in Inorganic Chemistry in 1986 at the University of Stuttgart. After a Postdoc period at the Max-Planck Institute for Metals Research in Stuttgart, he became Full Professor at the Institute of Materials Science at the Technical University of Darmstadt in 1993. He is an elected member of the World Academy of Ceramics, Fellow of the American Ceramic Society, the European Ceramic Society as well as Fellow of the School of Engineering at The University of Tokyo in Japan. Prof. Riedel was awarded the Gold Medal for Merits in Natural Sciences and an honorary doctorate of the Slovak Academy of Science as well as with the Gustav Tammann Prize of the German Society of Materials Science (DGM). He received honorary Professorships at the Tianjin University in Tianjin, China in 2009 and at the Xiamen University in Xiamen, China, in 2021. Prof. Riedel received the Innovation Talents Award of Shaanxi Province, China in 2019. He is Guest Professor at the University of Tokyo in the group of Prof. Ikuhara, Japan and was awarded with the International Ceramics Prize 2020 for "Basic Science" of the World Academy of Ceramics. He is Editor in Chief of the Journal of The American Ceramic Society and of Ceramics International. His current research interest is focused on two research areas, namely i) molecular synthesis of advanced structural and functional ceramics for ultra-high temperature and energy-related applications as well as ii) ultra-high pressure materials synthesis.